Dissolved iron and manganese in the Canadian Arctic Ocean: on the biogeochemical processes controlling their distributions

Manuel Colombo [a,*], Sarah L. Jackson [b, c], Jay T. Cullen [b], Kristin J. Orians [a]

[a] Department of Earth, Ocean, and Atmospheric Sciences, University of British Columbia, BC, V6T 1Z4, Canada
[b] University of Victoria, School of Earth and Ocean Sciences, 3800 Finnerty Road, Victoria BC, V8P 5C2 Canada
[c] Research School of Earth Sciences, The Australian National University, Canberra, Australian Capital Territory 0200, Australia
[*] Corresponding author: Department of Earth, Ocean, and Atmospheric Sciences, University of British Columbia, BC, V6T 1Z4, Canada. *Email: manuel.colombo@alumni.ubc.ca*

Abstract

Dissolved iron (DFe) and manganese (DMn) are essential micronutrients involved in vital phytoplankton physiological pathways, and their deficit can limit primary production in otherwise nutrient-replete surface ocean waters. In this work we present the spatial distributions and biogeochemical cycling of these metals across the Canadian GEOTRACES transect in the Canadian Arctic Ocean during the summer and autumn of 2015. Surface concentrations are dominated by freshwater inputs showing a strong negative correlation with salinity, especially for DMn which behaves more conservatively than DFe. The highest surface concentrations were measured in the Canadian Arctic Archipelago (Fe: 0.401-1.91 and Mn: 4.33-9.54 nmol kg^{-1}) and the Canada Basin (Fe: 0.225-0.479 and Mn: 3.93-7.02 nmol kg^{-1}), regions highly influenced by riverine inputs, whereas the lowest values were found in the Labrador Sea (Fe: 0.106-0.362 and Mn: 0.450-1.09 nmol kg^{-1}) where freshwater inputs diminished and phytoplankton uptake increased. Subsurface and deep water distributions for both metals are largely controlled by a complex balance between sources (advective inputs and organic matter remineralization) and removal processes. The subsurface peaks (~100-300 m) observed in the Canada Basin (Fe: 0.541±0.060 and Mn: 1.38±0.42 nmol kg^{-1}) and Baffin Bay (Fe: 0.753-1.03 nmol kg^{-1}) were advected from the Chukchi Sea and the Canadian Arctic Archipelago respectively, where DFe and DMn are released from the benthic boundary layer in these shelf-dominated environments. Advective sources associated with the Arctic Circumpolar Boundary Current, rather than vertical fluxes of DFe and DMn in

sinking particles, dominate metal distributions in the deep Canada Basin waters (>300 m). In the highly productive Baffin Bay and the Labrador Sea, organic matter remineralization is a notable source of DFe and DMn to deep waters. In the deepest waters (>1000 m), scavenging of DFe and DMn govern their vertical distributions; a pseudo-first order scavenging model explained the continuous removal of DMn in the Canada Basin, where the concentrations reach uniformly low concentrations (0.150±0.004 nmol kg^{-1}) after ~400 years. Applying this DMn scavenging model we were able to estimate the age (120-190 years) of deep Baffin Bay waters, a topic of discussion for many years.

***Keywords**:* Dissolved iron, Dissolved manganese, Trace metal biogeochemistry, Canadian Arctic Ocean, GEOTRACES

1 Introduction

Iron (Fe) and manganese (Mn) are key micronutrients, which along with major algal nutrients (e.g. nitrate, phosphate, silicic acid), regulate the biological productivity of global oceans and play a major role in the marine carbon cycle (Martin and Fitzwater, 1988; Bruland et al., 1991; Jickells et al., 2005; Boyd and Ellwood, 2010; Tagliabue et al., 2017). These micronutrients are involved in important phytoplankton metabolic pathways, such as photosynthesis (e.g. photosynthetic systems, the electron transport chain, activation of the ribulose l,5-bisphosphate carboxylase/oxygenase enzyme) and the nitrogen cycle (Maldonado and Price, 1996; Morel and Price, 2003; Morel et al., 2013), and they are also required by heterotrophic bacteria (Tortell et al., 1996; Morel et al., 2013). Understanding the mechanisms controlling the distributions of Fe and Mn in global oceans is therefore a primary endeavor of international programs such as GEOTRACES.

The Arctic Ocean can be viewed as a microcosm of the world ocean and as a natural laboratory where all the principle sources and sinks for metals of interest can be investigated. Atmospheric dust (dry and wet) deposition is an important external source of Fe and Mn to surface waters in the open ocean (Duce et al., 1991; Martin J.H., Gordon M.R., 1991; Guieu et al., 1994; Jickells et al., 2005; Moore and Braucher, 2008). More recently, riverine inputs, sediment-water interactions, continental margin inputs and hydrothermal vents are being recognized as significant source terms in the biogeochemical cycles of Fe and Mn (Fung et al., 2000; Lam and Bishop, 2008; Middag et al., 2011b; Klunder et al., 2012a; Jeandel and Oelkers, 2015; Jeandel, 2016; Fitzsimmons et al., 2017; Milne et al., 2017; Tagliabue et al., 2017; Cheize et al., 2019). The Arctic Oceans high latitude, remote location and extensive seasonal sea ice cover tend to attenuate and modulate atmospheric fluxes (Marsay et al., 2018b; Shelley et al., 2018). The Arctic receives impressive freshwater inputs (~11% of world's river discharge) and plays host to expansive continental shelves, both characteristics that predict significant sources of Fe and Mn (Lammers et al., 2001; Hölemann et al., 2005; Measures et al., 2008; Pokrovsky et al., 2010; Bring et al., 2016). Despite these large source terms, Fe and Mn are usually found at sub-nanomolar levels in the

dissolved phase owing to rapid biological uptake in surface waters, precipitation of Fe^{+3} and $Mn^{+3/4}$ oxides and oxyhydroxides in oxygenated waters, and scavenging onto organic and inorganic particles throughout the water column (Landing and Bruland, 1987; Johnson et al., 1997; Sunda, 1997; Wu et al., 2001; Morgan, 2005; Klunder et al., 2011; Bown et al., 2018). The low solubility of Fe^{3+} in oxygenated seawater dictated by thermodynamics, is countermanded through its complexation and stabilization in solution by organic ligands, which account for approximately 99.9% of the DFe observed in ocean waters (Rue and Bruland, 1995; Gerringa et al., 2015). More recently, Oldham et al. (2017) reported the presence of organic ligands stabilizing Mn^{+3}, otherwise insoluble in ocean waters, and indicating that ligands may play a greater role in governing DMn distributions. Investigations of the Fe and Mn biogeochemistry in the Arctic therefore has the potential to provide important insights in the rates and nature of key processes controlling the cycling of these essential metals in the marine environment.

Since the launch of GEOTRACES in 2010 (http://www.geotraces.org/), our knowledge about the concentrations, biogeochemical cycles and processes shaping the distributions of DFe and DMn has significantly increased. High resolution profiles of DFe and DMn have been sampled on transects across major ocean basins, and in remote areas of the Southern Atlantic Ocean and the Arctic Ocean (Wu et al., 2014; Fitzsimmons et al., 2015; Hatta et al., 2015; Hulten et al., 2017; John et al., 2018; Pham and Ito, 2018; Schlitzer et al., 2018). Even though numerous studies on Fe and Mn biogeochemistry in the Arctic Ocean have been published in the last 10 years, they have focused on the Eurasian Basin (Middag et al., 2011b; Klunder et al., 2012b; Klunder et al., 2012a), the Chukchi Sea and adjacent shelf break areas of the Canada Basin (Nakayama et al., 2011; Aguilar-Islas et al., 2013; Hioki et al., 2014; Kondo et al., 2016). In this manuscript we report the concentrations of DFe and DMn in the Canada Basin, the Canadian Arctic Archipelago, Baffin Bay and the Labrador Sea elucidating the mechanisms controlling the spatial distributions of these elements in this key region, where Arctic waters properties are modified and ultimately exported to the North Atlantic Ocean.

2 Study Area and Hydrography

The Canada Basin is strongly salinity stratified, with a polar mixed layer (PML), seasonally modified by freeze-thaw cycles of ice and snow, and a multilayered halocline (~30-400 m) insulating the PML from the underlying saltier and warmer Atlantic Layer (AL). The halocline assembly consists of the Alaskan Coastal Water (ACW), with a potential temperature (θ) of about ~0 °C and a salinity (S) range of 30 <S< 32, and the winter Bering Sea Water (wBSW), distinguished by a shallow temperature minimum near S= 33.1, which are advected from Bering Strait and contribute to the upper and middle halocline layers (Steele et al., 2004; McLaughlin et al., 2005; Timmermans et al., 2017; Figures 1 and 2a). Unlike the upper and middle halocline, the lower halocline (LH) consists mostly of Atlantic-origin waters, and is identified by a sharp increase in temperature at salinities between 33.3 and 34.6 (McLaughlin et al., 2005; Shimada et al., 2005; Woodgate and Aagaard, 2005). The AL (~400-1200 m) has two components: the Fram Strait Branch (FSB), distinguished by a temperature maximum and the Barents Sea Branch (BSB), which is deeper and colder (Smethie et al., 2000; McLaughlin et al., 2004; Aksenov et al., 2011). Underlying the AL lies the old, cold and more saline Canada Basin Deep Water (CBDW > 1200 m; Timmermans et al., 2003; Figs. 1 and 2a).

The Canadian Arctic Archipelago (CAA) is a complex network of islands and shallow straits, connecting the Arctic Ocean to Baffin Bay. This shelf dominated region is an important export conduit for fresh and nutrient rich Pacific waters to the North Atlantic, enhancing the productivity downstream (Michel et al., 2006; Beszczynska-Möller et al., 2011; Wang et al., 2012; Hill et al., 2013). The CAA links the Arctic Ocean with Baffin Bay by three main pathways, Parry Channel (~120 m), running from M'Clure Strait to Lancaster Sound, Nares Strait (~ 220 m), and Jones Sound (~125 m). Two main domains are recognized in the CAA based on the conductivity, temperature and depth (CTD) data. The Arctic water of Pacific origin, which are cooler ($-1.6<\theta<0.8$ °C) and fresher ($25.1<S<34.8$), dominate the western CAA region and the southern side of Parry Channel (CB1, CAA4 and CAA7-9), compared to

Baffin waters of Atlantic origin (-1.5<θ<4.9 °C; 28.2<S<34.5) which recirculate in the eastern CAA (CAA1-3 and CAA5; Figs. 1 and 2b).

Baffin Bay is connected to the Labrador Sea and the North Atlantic Ocean through Davis Strait (~650 m). The overall circulation in this bay is cyclonic, with a northward flow on the eastern side of Davis Strait, the West Greenland Current (WGC), which consists of subsurface fresh waters of Arctic origin (East Greenland Current), and the warm and salty West Greenland Intermediate Water (WGIW: ~300-800 m; θ> 1.3 °C and S> 34.2) of North Atlantic origin (Cuny et al., 2005; Curry et al., 2011; Lozier et al., 2017). This northward inflowing water is modified during its cyclonic circulation, and the upper layers of the WGC are mixed with Arctic waters, resulting in the fresh and cold Arctic Water (AW; θ< 0 °C and 32.0 <S< 33.7), which continues its flow to the Labrador Sea as the Baffin Current (Tang et al., 2004; Cuny et al., 2005). Underlying the WGIW, lies the Baffin Bay Deep Water (BBDW), which is characterized by a small change in salinity and a constant decrease in potential temperature (Tang et al., 2004; Figs. 1 and 2c).

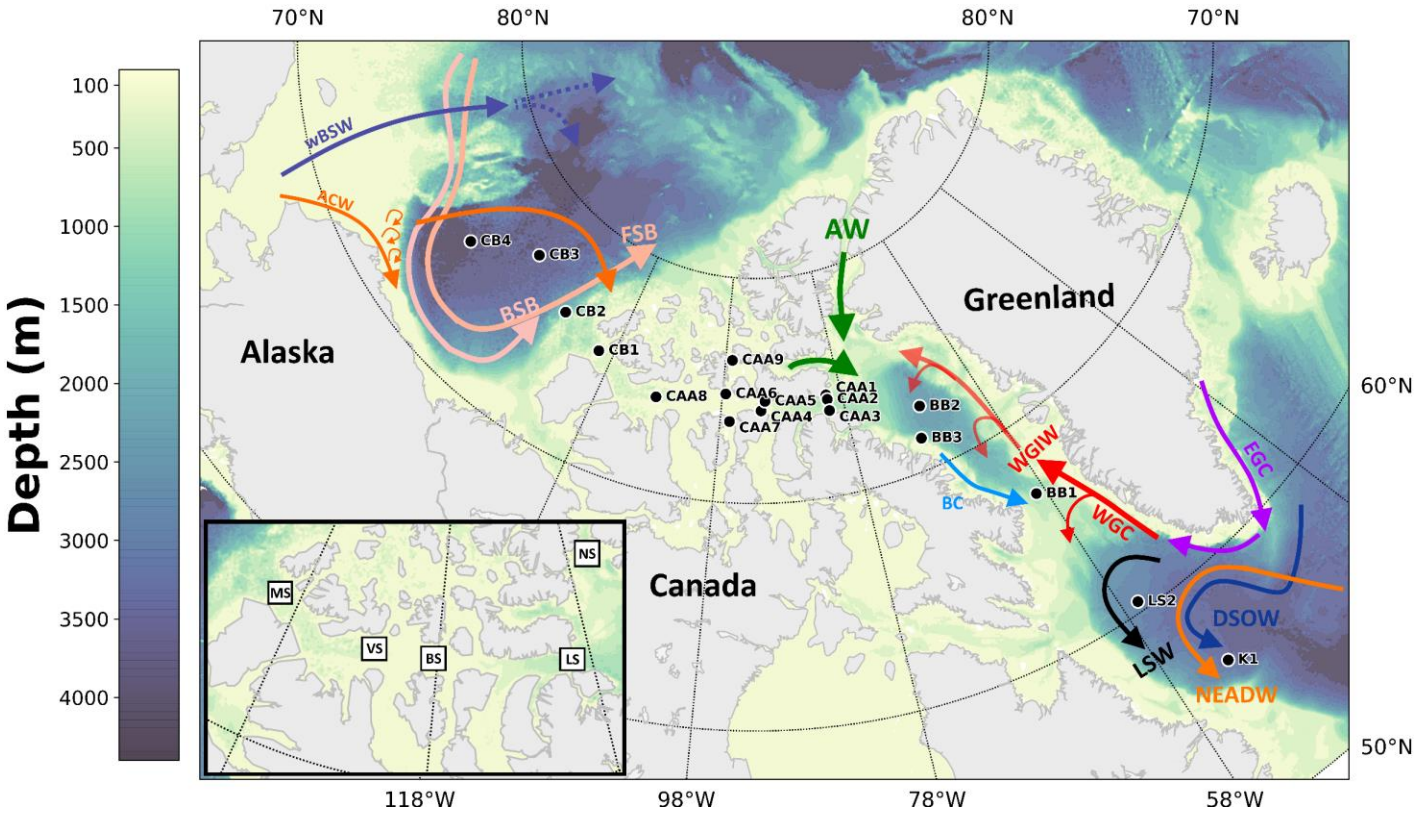

Fig. 1. Sampled stations for Fe and Mn during the Canadian Arctic GEOTRACES cruises (GN02 and GN03), bathymetry and schematic of water circulation in the Canada Basin (after Aksenov et al., 2011; Kondo et al., 2016) and Baffin Bay and the Labrador Sea (after Yashayaev and Clarke, 2008; Curry et al., 2011; Lozier et al., 2017). ACW: Alaskan Coastal Water, wBSW: winter Bering Sea Water, FSB: Fram Strait Branch, BSB: Barents Sea Branch, AW: Arctic Water, EGC: East Greenland Current, WGC: West Greenland Current, WGIW: West Greenland Intermediate Water, BC: Baffin Current, LSW: Labrador Sea Water, NEADW: Northeast Atlantic Deep Water, DSOW: Denmark Strait Overflow Water. Canada Basin stations: CB2-CB4, Canadian Arctic Archipelago stations: CB1and CAA1-CAA9, Baffin Bay stations: BB1-BB3, Labrador Sea stations: LS2 and K1. Landmarks and straits of the Canadian Arctic Archipelago are displayed in the inset, MS: M'Clure Strait, VS: Viscount Melville Sound, BS: Barrow Strait, LS: Lancaster Sound and NS: Nares Strait. A detailed view of the Canadian Arctic Archipelago is also presented in Fig. 9a.

The subsurface circulation in the Labrador Sea is cyclonic, consisting of two components: the WGC and the Labrador Current, which flows southward along the Labrador Shelf and Slope and is the extension of the Baffin Current (BC; Cuny et al., 2002; Fischer et al., 2004). The Labrador Sea Water (LSW) lies between the subsurface water and the deep west boundary current; two LSW classes were distinguished from the CTD in 2015: the newly ventilated and fresher LSW formed during the winters of 2014 and 2015 (LSW-2015), and the old, saltiest and least oxygenated LSW produced in the winters of 1987-1994 (LSW-87/94; Yashayaev and Loder, 2016). Underlying the LSW-87/94, lies the saline, warm (θ ~3 °C, S ~34.92) and less oxygenated Northeast Atlantic Deep Water (NEADW), and the deepest, less

saline, colder ($\theta \leq 2.6$ °C, S ~ 34.9), and more-recently oxygenated Denmark Strait Overflow Water (DSOW; Yashayaev et al., 2007; Yashayaev and Loder, 2016; Figs. 1 and 2d).

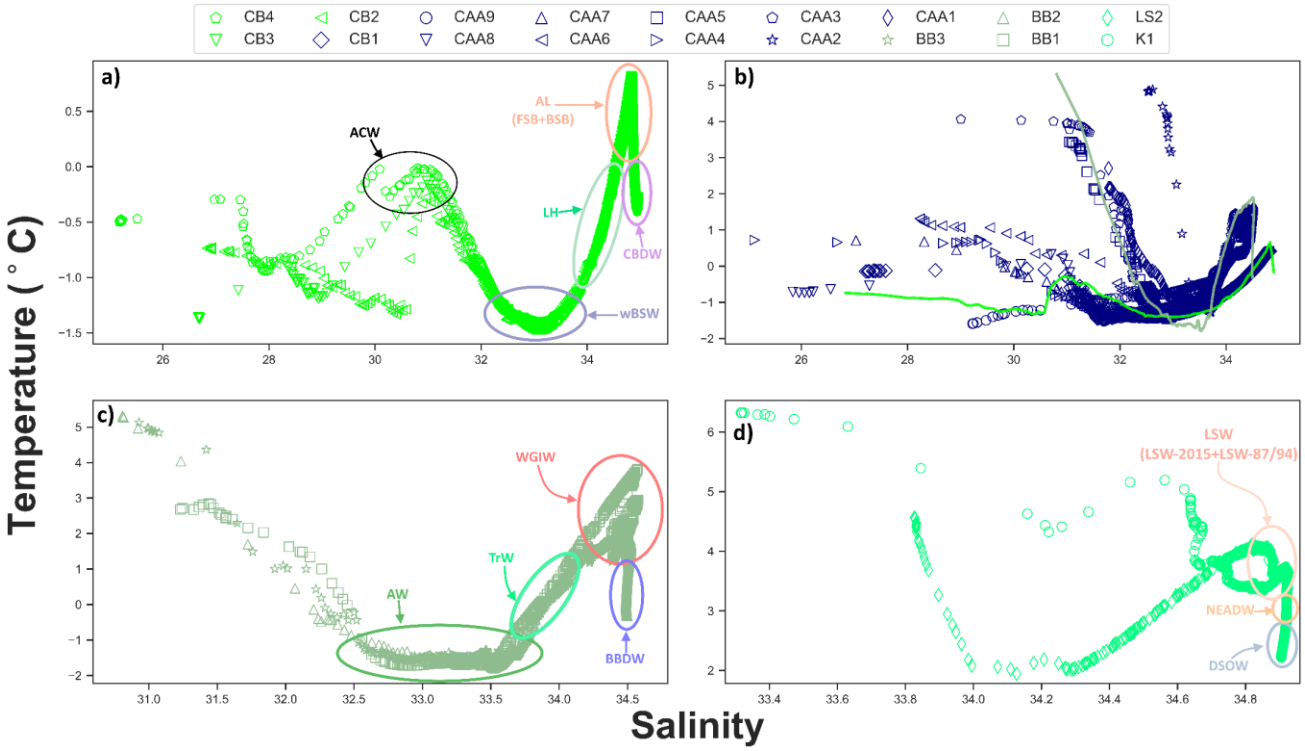

Fig. 2. Potential temperature (θ) versus salinity (S) diagram for the Canada Basin (a), the CAA (b), Baffin Bay (c) and the Labrador Sea (d). For the CAA (b), the θ/S data from the Canada Basin endmember (CB2) and Baffin Bay endmember (BB2) are shown with solid lines. The main water masses are indicated in the figure: ACW: Alaskan Coastal Water, wBSW: winter Bering Sea Water, LH: Lower Halocline, AL: Atlantic Layer, FSB: Fram Strait Branch, BSB: Barents Sea Branch, CBDW: Canada Basin Deep Water, AW: Arctic Water, TrW: transitional water, WGIW: West Greenland Intermediate Water, BBDW: Baffin Bay Deep Water, LSW: Labrador Sea Water, NEADW: Northeast Atlantic Deep Water, DSOW: Denmark Strait Overflow Water.

3 Methods

3.1 Sample collection

Seawater samples were collected on the *CCGS Amundsen* as part of GEOTRACES sections GN02 and GN03 (10/07/2015-1/10/2015) which covered an area from 56°N to 77°N and 53°W to 150°W in the Canadian Arctic. The sampling was carried out during summer early fall months, and hence, most stations were ice-free when seawater samples were collected; a map displaying sea ice concentrations in the study area in the summer of 2015 is presented in the Supplementary Material (Electronic Annex, Fig. EA1).

Vertical profiles of 8 to 25 discrete depths were obtained at 18 stations: three in the Canada Basin, ten in the CAA, three in Baffin Bay and two in the Labrador Sea (Fig. 1). A trace-metal clean sampling system consisting of a powder-coated aluminium frame, which held twelve 12 L Teflon-coated GO-FLO bottles (General Oceanics, Miami FL USA) and a SeaBird 911 CTD/SBE 43 oxygen sensor instrument package (Seabird Electronics Inc, Bellevue WA USA), attached by a 4000 m 4-member conducting Vectran cable encased in polyurethane (Cortland Cable Co., Cortland NY USA) was used to collect seawater samples. On-board the ship, samples were gravity-filtered through 0.2µm Acropak filters (Pall Corporation) into 250 and 500 mL LDPE bottles (Bel Art and Nalgene) in a HEPA filtered air environment. The sampling devices and bottles were prepared and pre-cleaned according to established GEOTRACES protocols (Cutter et al., 2010). After filtration, samples were acidified to pH=1.7 using SeaStar trace metal grade hydrochloric acid (SeaStar Chemicals, Sidney, BC).

3.2 Trace metal analyses

Dissolved Fe and Mn from the Canadian Arctic GEOTRACES program were both measured independently by labs at the University of British Columbia (UBC) and the University of Victoria (UVic) following different analytical procedures. To prevent contamination, the processing and analysis of the samples at UBC and UVic were conducted in class 1000 laboratories, pressurized with HEPA filtered air, and under class 100 laminar flow fume hoods. All the plasticware used during the sample preparation and analysis were cleaned according to GEOTRACES protocols (Cutter et al., 2010).

3.2.1 Magnesium-induced coprecipitation and isotope dilution method (UBC)

Dissolved Fe and Mn were preconcentrated 50-fold from 50 mL acidified seawater using a modified magnesium-induced coprecipitation method and quantified by isotope dilution (Wu and Boyle, 1998; Saito and Schneider, 2006; Colombo et al., 2019b). As the scavenging efficiency of Mn, a monoisotopic element, is similar to Fe, DMn concentrations can be quantified by normalization to ^{57}Fe counts:

$Mn = \left[\frac{[Mn]_{cps}}{[^{57}Fe]_{total\ cps} - [^{57}Fe]_{sample\ cps}}\right] x \left[Fe_{spike}\right] x \left[\frac{spike\ volume}{total\ volume}\right] x \left[\frac{Fe\ sensitivity}{Mn\ sensitivity}\right]$ as described by Saito and Schneider (2006). The seawater samples were equilibrated overnight with ^{57}Fe enriched spikes (Oak Ridge National Laboratories) and trace metals were then precipitated with high-purity NH_4OH (Seastar Baseline Chemicals Inc., Sidney, Canada). The analyses were conducted by high resolution Thermo Finnigan Element2 Inductively Coupled Plasma Mass Spectrometry in the Pacific Centre for Isotopic and Geochemical Research at UBC. A medium mass resolution was selected for Fe and Mn analysis in order to remove isobaric interferences caused by $^{40}Ar^{16}O$ and $^{40}Ca^{16}O$ for ^{56}Fe and $^{15}N^{40}Ar$ for ^{55}Mn. The counts per second (cps) of the blanks run during the analysis (n=69) represented only 1.5±1.1 (0.011±0.006 nmol kg^{-1}) and 3.0±1.9% (0.065±0.012 nmol kg^{-1}) of sample cps for Fe and Mn, respectively.

3.2.2 Offline extraction and triple quadrupole ICP-MS/MS method (UVic)

Dissolved Fe and Mn were extracted and preconcentrated (8x) using the *seaFAST*-pico SC-4 DX system (ESI, Omaha, NE, USA). For each sample 20 mL of seawater was loaded onto a column which contained Nobias PA-1 resin (with functional groups ethylenediaminetriacetic acid and iminodiacetic acid). To remove the seawater matrix, the column was then rinsed with an ammonium acetate buffer solution (pH=6.0) prepared by bubbling high-purity anhydrous ammonia gas through twice-distilled acetic acid with the pH adjusted by additions of NH_3. Samples were eluted in 2.5 mL of 1.6 M Seastar Baseline HNO_3 (Seastar Chemicals, Sidney, BC, Canada). The preconcentrated samples were analysed using the Agilent 8800 ICP-MS/MS (Jackson et al., 2018). This method yielded a limit of detection of 0.029 and 0.002 nmol L^{-1} for Fe and Mn, respectively.

3.2.3 Quality control and accuracy

During the analysis, procedural blanks and quality control spikes (acidified Milli-Q water equilibrated with natural trace metal standards) were routinely run to ensure quality of the measurements. The accuracy was calculated by analyzing the SAFe S, SAFe D1, SAFe D2 and GSP S GEOTRACES

reference materials multiple times, and the results were all within the error of the reported values from the oceanographic community (Table EA1). The precision of the analysis, relative standard deviations (1RSDs) of SAFe D1, D2 and GSP reference materials, was 4.3±1.4 and 3.7±1.4% for Fe and Mn, and the RSDs of replicate analysis of control spikes (n=40) run by the UBC group were 3.4 and 4.4% from Fe and Mn. Additionally, the intercalibration exercises carried out with the Texas A&M University were in close agreement to our values (Figs. EA2 and EA3).

The sample concentrations reported here were corrected for the analytical blank by subtracting the average blank on the corresponding analytical day. The DFe and DMn results from UBC and UVic (replicate samples stored in different LDPE bottles) showed excellent agreement (Figs. EA2 and EA3), and therefore the two data sets were combined (Tables EA2 and EA3). The statistical analysis and graphics in this manuscript were developed using Python 3.6.0.

4 Results

This study reports the vertical and spatial distributions of dissolved Fe and Mn concentrations in the Labrador Sea, Baffin Bay, the Canadian Arctic Archipelago and the Canada Basin. The full dataset of DFe and DMn is presented in Tables EA2 and EA3. Interpolated contour sections of DFe and DMn across the studied basins are presented in Figs. 3, 4 and 5, along with the full depth profiles for each station. All sampled stations are displayed in a single figure in the supplementary material (Fig. EA4).

In general, surface DFe and DMn concentrations were high in the Canada Basin and the Canadian Arctic Archipelago (CAA), decreasing their concentrations towards the Labrador Sea. Below surface waters, the lowest DFe concentrations were measured in the Canada Basin (0.238-0.616 nmol kg^{-1}), followed by the Labrador Sea (0.114-0.827 nmol kg^{-1}) and Baffin Bay (0.529-2.00 nmol kg^{-1}), while the CAA displayed the highest Fe concentrations (0.436-6.87 nmol kg^{-1}; Figs. 3a, 4 and EA4). Similar to DFe, the highest subsurface DMn concentrations were measured in CAA (0.416-8.40 nmol kg^{-1}), while

deep water concentrations were low and similar across the Canada Basin, Baffin Bay and the Labrador Sea (Figs. 3b, 5 and EA4).

In this paper we first discuss the biogeochemical and physical processes affecting the distributions of DFe and DMn in the surface waters of the Canadian Arctic Ocean (<40 m), followed by subsurface (~40-300 m) and deep waters (>3000 m).

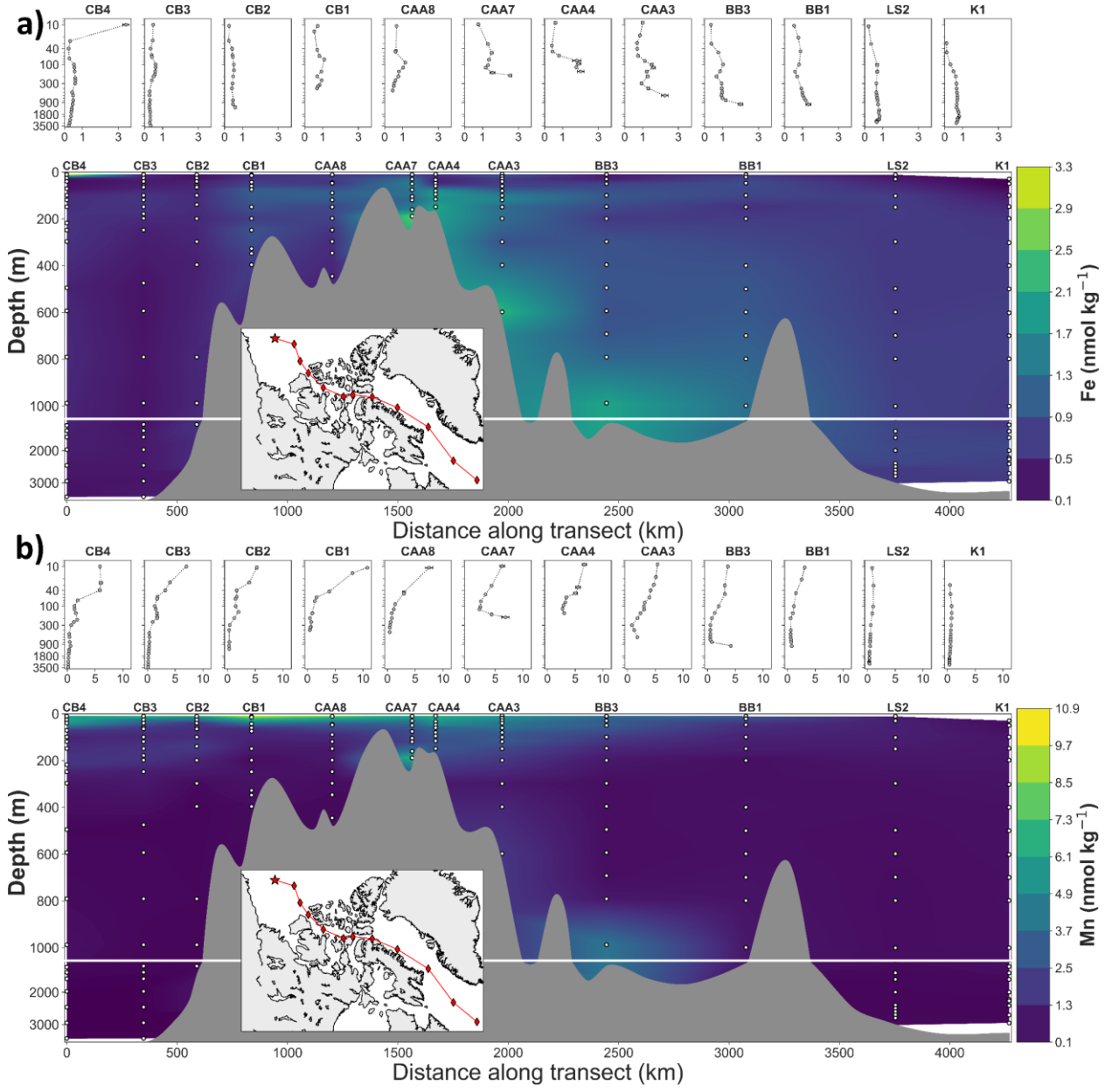

Fig. 3. Interpolated contour section of dissolved Fe (a) and Mn (b) along the Canada Basin, the Canadian Arctic Archipelago, Baffin Bay and the Labrador Sea. Sampled depths are superimposed on the plot (white circles) and the individual profiles are displayed above each contour plot. Error bars for individual profiles reflecting the standard deviation of replicate

analyses are usually smaller than the symbols. Stations included are displayed in the inset map and the beginning of the transect is indicated by the red star. Note the break axis in the contour map (white line at 1050 m) and the logarithmic scale for the individual profiles. Stations were chosen to capture the flow of Arctic waters from the Canada Basin to the Labrador Sea.

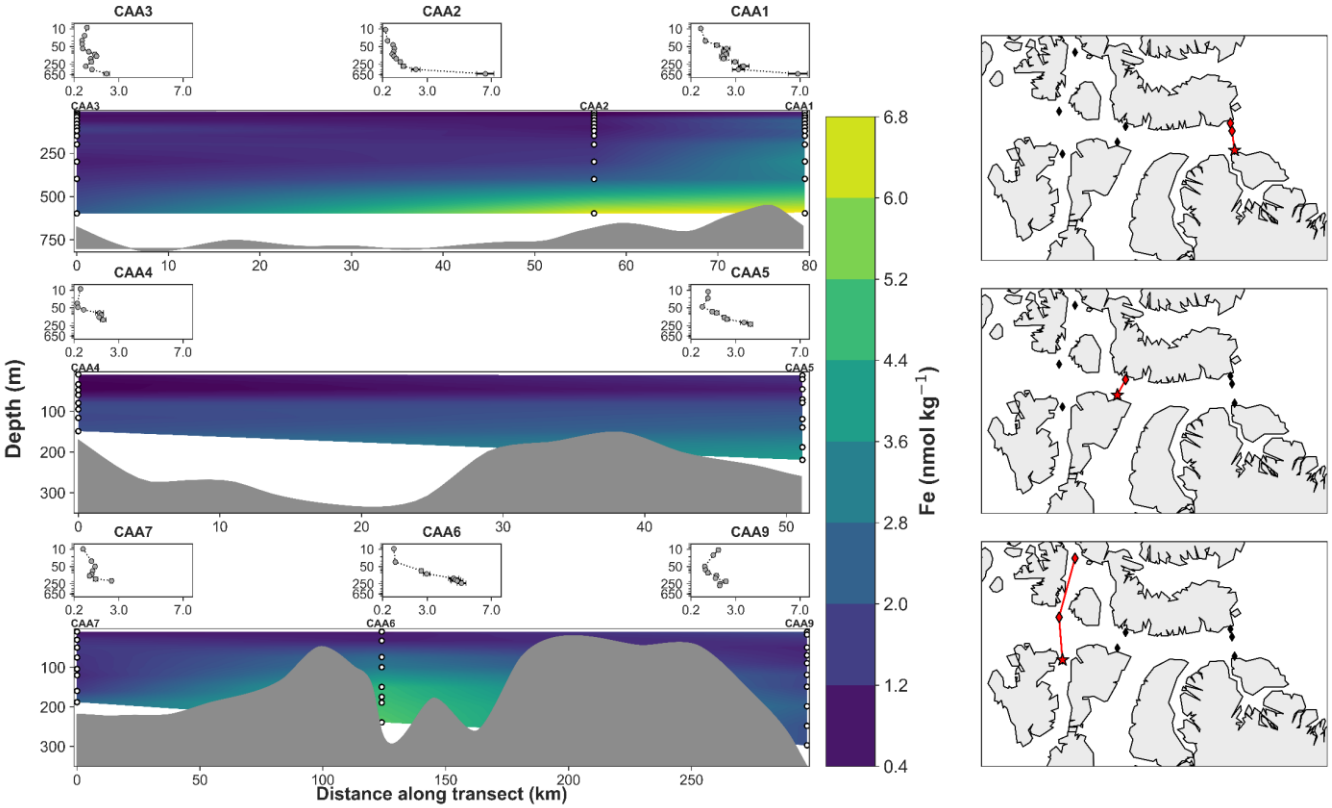

Fig. 4. Interpolated contour section of dissolved Fe in the Canadian Arctic Archipelago (CAA) across Parry Channel; sampled depths are superimposed in the plot (white circles) and the individual profiles are displayed above each contour plot. Error bars for individual profiles reflecting the standard deviation of replicate analyses are usually smaller than the symbols. For a larger view of individual CAA profiles please see Fig. 9a. The stations sampled at the three transects across Parry Channel are displayed in the maps, the beginning of the transect is indicated by the red star (Southern side of Parry Channel). Note the logarithmic scale for the individual profiles.

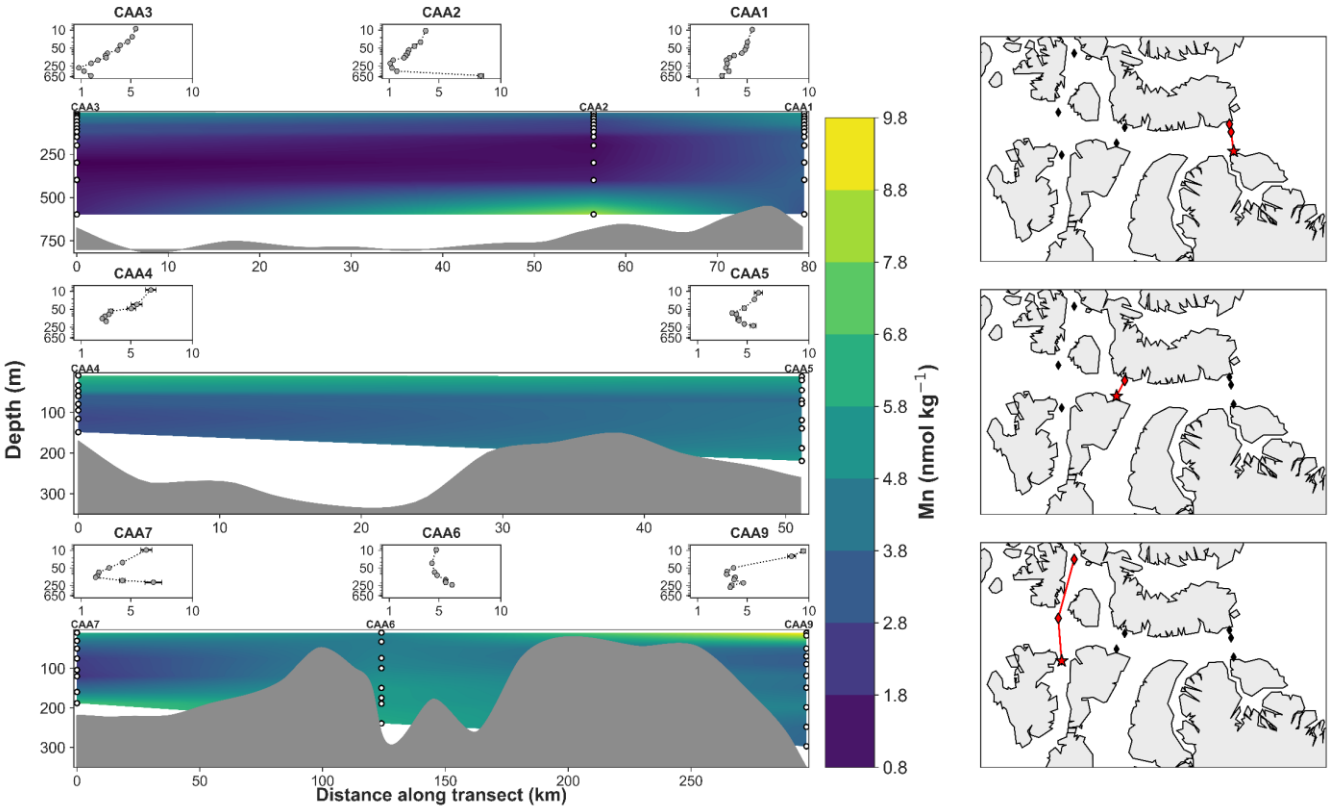

Fig. 5. Interpolated contour section of dissolved Mn in the Canadian Arctic Archipelago (CAA) across Parry Channel; sampled depths are superimposed in the plot (white circles) and the individual profiles are displayed above each contour plot. Error bars for individual profiles reflecting the standard deviation of replicate analyses are usually smaller than the symbols. For a larger view of individual CAA profiles please see Fig. 9a. The stations sampled at the three transects across Parry Channel are displayed in the maps, the beginning of the transect is indicated by the red star (Southern side of Parry Channel). Note the logarithmic scale for the individual profiles.

4.1 Dissolved Fe and Mn in surface waters

For most stations, the highest DMn concentrations were measured in the upper 40 m (3.10-10.78 nmol kg^{-1}), sharply decreasing with increasing depth (Figs. 3b, 5 and 6). Intermediate concentrations were found in Canada Basin surface waters (<40 m; 5.15±1.21 nmol kg^{-1}), while distinctively high concentrations were present in M'Clure Strait (CB1), Viscount Melville Sound (CAA8) and Penny Strait (CAA9) in the western region of the CAA (8.91±1.15 nmol kg^{-1}). The concentrations then decrease towards Barrow

Strait (CAA4 to CAA7) and Lancaster Sound (CAA1 and CAA3) in the eastern CAA (5.32±0.66 nmol kg^{-1}), and Baffin Bay (3.26±0.38 nmol kg^{-1}; Fig. 6). Lowest surface water concentrations were found in the Labrador Sea (0.795±0.263 nmol kg^{-1}).

Surface DFe concentrations were generally low (0.106-1.91 nmol kg^{-1}) in the Canadian Arctic Ocean, with the exception of CB4 where extremely high concentrations (3.42±0.19 nmol kg^{-1}) were measured in the polar mixed layer (Figs. 3a, 4 and 6). Although there was more variability than observed for DMn, surface (<40 m) DFe distributions resemble the general trends described for DMn. The highest concentrations were measured in the CAA (1.12±0.34 nmol kg^{-1}); however, stations CB1, CAA8 and CAA4 had lower surface DFe values (0.587±0.113 nmol kg^{-1}) despite high DMn concentrations measured at these stations, reflecting either different sources and/or removal mechanisms for these metals (Fig. 6). Intermediate DFe concentrations were measured in Baffin Bay (0.336-0.763 nmol kg^{-1}), followed by the Canada Basin (0.225-0.479 nmol kg^{-1}; not including PML value at CB4) and the Labrador Sea (0.106-0.362 nmol kg^{-1}).

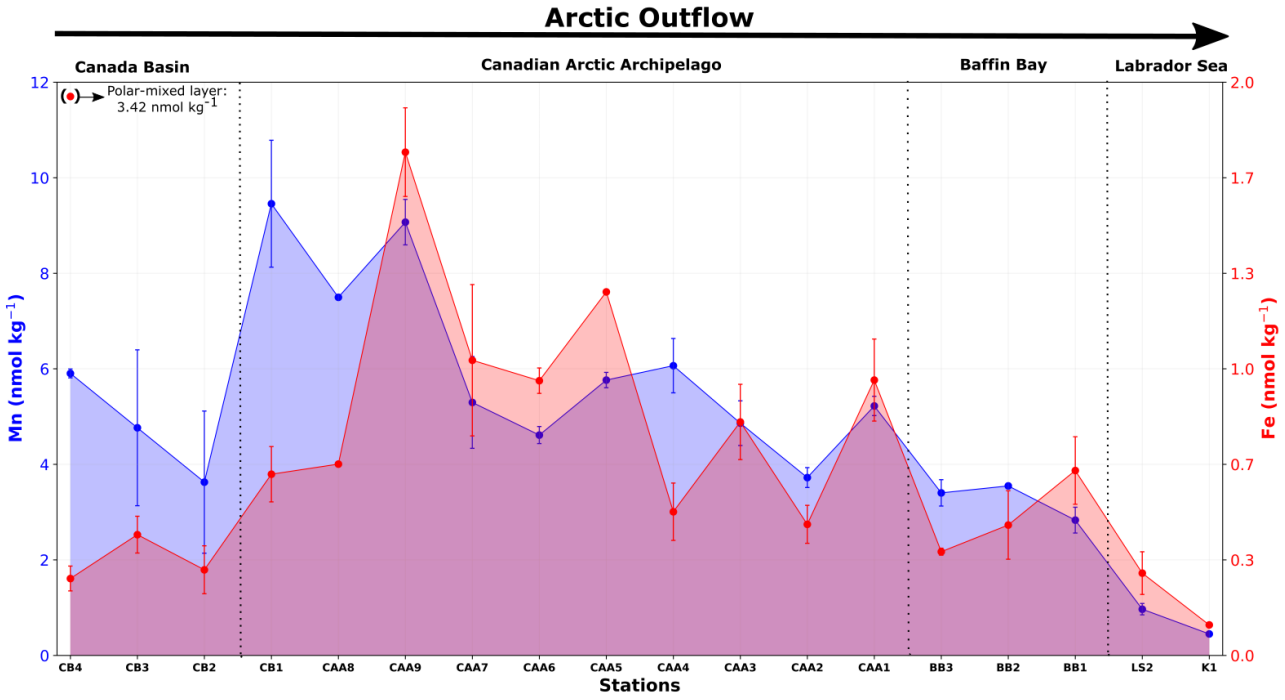

Fig. 6. Average and standard deviation (1SD) surface (< 40 m) DFe and DMn concentrations for the stations sampled across the Canada Basin, Canadian Arctic Archipelago, Baffin Bay and the Labrador Sea. The error bars reflecting the standard deviation for stations CB4 (Mn: 5.90±0.09 nmol kg^{-1}), CAA5 (Fe: 1.27±0.004 nmol kg^{-1}), BB3 (Fe: 0.362±0.012 nmol kg^{-1}) and

BB2 (Mn: 3.55±0.03 nmol kg^{-1}) are smaller than the symbols. For CAA8 and K1 stations, one sample was collected within 0-40 m depth range.

4.2 Dissolved Fe and Mn in shelf seas and subsurface waters

In this section, we present the distributions of DFe and DMn in the CAA shelf dominated region (stations CB1 and CAA1-CAA9) and in subsurface waters (40-300 m) in the Canada Basin, Baffin Bay and the Labrador Sea, focusing on the advective features found in these deep basins.

The Canadian Arctic Archipelago (CAA). The highest concentrations of DFe and DMn in the Canadian Arctic Ocean were generally found in the CAA, though a marked spatial difference is noted between western and eastern CAA (Figs. 3, 4 and 5). In M'Clure Strait and Viscount Melville Sound (CB1 and CAA8) the concentrations of DMn were lower than the rest of CAA stations, steadily decreasing from 40 to 200 m and remaining low approaching the seafloor (0.549±0.092 and 0.545±0.145 nmol kg^{-1}, respectively), whereas east of Barrow Strait (sill depth ~120 m) the concentrations were up to an order of magnitude higher. Likewise, DFe concentrations were lower in M'Clure Strait and Viscount Melville Sound and the vertical profiles were different from the eastern CAA stations, with an increase of DFe below surface waters, peaking between 70-100 m (CB1: 1.10±0.05 and CAA8: 1.15±0.02 nmol kg^{-1}), and steadily decreasing towards the bottom (CB1: 0.688±0.008 and CAA8: 0.447±0.036 nmol kg^{-1}; Fig. 3a). In the eastern CAA, below 40 m, DMn concentrations generally decreased with depth to near-bottom waters where a rapid rise of Mn was detected. The stations located along the southern edge of Parry Channel (CAA7, CAA4 and CAA3) exhibited lower subsurface concentrations (2.55±0.42, 3.06±0.83 and 2.57±1.03 nmol kg^{-1}, respectively) than the stations located on the north side of Parry Channel and in Penny Strait (CAA6: 5.23±0.39, CAA5: 4.28±0.32, CAA1: 3.85±0.66 and CAA9: 3.84±0.40 nmol kg^{-1}; Fig. 5). An increase of DMn was observed in near-bottom waters for most stations in the eastern CAA, with higher concentrations found at stations along the northern edge of Parry Channel (CAA6: 6.06±0.12, CAA5: 5.51±0.22 and CAA2: 8.40±0.23 nmol kg^{-1}), compared with the southern edge stations (CAA4: 3.02±0.12 and CAA3: 1.78±0.04 nmol kg^{-1}). However, CAA7 displayed concentrations comparable to the northern stations (6.84±0.66 nmol kg^{-1}; Fig. 5).

Contrasting with DMn distribution in the eastern CAA, DFe concentrations, below 40 m, generally increased with depth to near-bottom waters. As was observed for DMn in near-bottom waters, much higher DFe was measured in the northern Parry Channel (CAA6: 5.13±0.27, CAA5: 3.91±0.14, CAA2: 6.62±0.54 and CAA1: 6.87±0.60 nmol kg^{-1}) compared to the southern stations (CAA7: 2.54±0.091, CAA4: 2.01±0.19 and CAA3: 2.24±0.18 nmol kg^{-1}; Fig. 4). Station CAA2 stands out for having significantly (*p-value*< 0.01) lower concentrations of DFe and DMn compared to CAA1, despite being only ~20 km distant from CAA1 (Figs. 4 and 5).

The Canada Basin. Below the surface maximum, DMn concentrations decreased sharply with depth, reaching a subsurface minimum at ~100 m (1.35±0.08 nmol kg^{-1}), while DFe concentrations remained similar (0.396±0.060 nmol kg^{-1}) from the surface down to 100 m (Figs. 3 and 7). From about 100 to 300 m a distinctive feature of high concentrations for both DFe and DMn was observed in the density range of σ_θ= 25.69-27.64, reaching values as high as 0.616 and 2.00 nmol kg^{-1}, respectively. These subsurface peaks were consistent across the Canada Basin (Fe: 0.541±0.060 and Mn: 1.37±0.41 nmol kg^{-1}), with no significant differences in the concentrations detected among the three stations in this basin (ANOVA; *p-value*> 0.05; Figs. 3 and 7).

Baffin Bay and the Labrador Sea. Dissolved Fe in subsurface Baffin Bay waters exhibited a distinctive peak within the AW, with the highest values observed at BB3 (0.884±0.108 nmol kg^{-1}) along the Baffin Bay slope, while the peaks were less pronounced in central Baffin Bay (BB2: 0.624±0.079 nmol kg^{-1}) and Davis Strait (BB1: 0.754±0.117 nmol kg^{-1}). In the Labrador Sea this subsurface maximum was not observed, but a sharp rise of DFe was noted from the surface to 300 m (σ_θ~ 27.7) at stations LS2 and K1 (0.287±0.148 to 0.652±0.033 and 0.106±0.038 to 0.652±0.037 nmol kg^{-1}, respectively; Figs. 3a and 7). In contrast, in Baffin Bay DMn did not show a subsurface peak, and the concentrations rapidly decreased with depth reaching consistently low concentrations at ~300 m (σ_θ~ 27.4; 0.500±0.064 nmol kg^{-1}). Dissolved Mn in Labrador Sea subsurface waters was slightly higher than surface waters, related to the pronounced reduction of freshwater inputs

and enhanced phytoplankton uptake of DMn in this basin (section 5.1), slowly decreasing its concentration with depth to approximately 300 m (LS2: 0.590±0.050 and K1: 0.665±0.018 nmol kg^{-1}).

4.3 The contrasting biogeochemistry of DFe and DMn in deep waters

Inter-basin differences of DFe and DMn were observed in the deep waters (>300 m; Figure 3), with the lowest values found in the Canada Basin (Fe-AVG: 0.361±0.086, Fe-range: 0.238-0.592 nmol kg^{-1}; Mn-AVG:0.280±0.101, Mn-range: 0.147-0.565 nmol kg^{-1}), followed by the Labrador Sea (Fe-AVG: 0.717±0.052, Fe-range: 0.647-0.827 nmol kg^{-1}; Mn-AVG:0.428±0.095, Mn-range: 0.306-0.593 nmol kg^{-1}), while Baffin Bay had the highest values (Fe-AVG: 0.942±0.151, Fe-range: 0.647-1.330 nmol kg^{-1}; Mn-AVG:0.485±0.176, Mn-range: 0.239-0.776 nmol kg^{-1}).

The Canada Basin. An interesting difference in DFe distributions was observed in the Canada Basin below 300 m, where significantly (*p-value*< 0.01) lower concentrations were measured at CB3 station than at the stations CB2 and CB4 across FSB, BSB, CBDW (σ_θ> 27.92), a phenomenon which was not seen for DMn (Fig. 7). Below the subsurface peak of Fe and Mn in the wBSW, concentrations dropped within the Atlantic Layer (AL), from approximately 300 to 800 m, and the lowest levels of DFe (CB2 and CB4: 0.412±0.007; CB3: 0.284±0.001 nmol kg^{-1}) and DMn (CB2-CB4: 0.327±0.012 nmol kg^{-1}) coincided with the FSB warm core (θ= 0.7-0.8 ºC) at ~500 m (σ_θ= 27.92; Fig. 7). In the lower AL, across BSB waters (~800-1000 m), concentrations increased slightly, while in the CBDW (>1200 m), DMn concentrations decreased steadily to the bottom with uniformly low concentrations below 2500 m (CB3: 0.149±0.002 and CB4: 0.158±0.006 nmol kg^{-1}). Similarly, DFe at CB4 decreased steadily from 1000 to 3500 m (0.449±0.003 to 0.238±0.011 nmol kg^{-1}), while at CB3, DFe distributions were maintained virtually uniform in CBDW (0.303±0.024 nmol kg^{-1}; Fig. 7).

Baffin Bay. Dissolved Fe concentrations rose from transitional waters (TrW, 0.669±0.019 nmol kg^{-1}) across the warm (1.3-3.9 ºC) West Greenland Intermediate Water (WGIW) to ~1000 m, where similar concentrations were measured from 300 to 800 m at the stations BB3 and BB1 along the Baffin Bay slope (0.995±0.082 and 1.09±0.13 nmol kg^{-1}), and slightly lower concentrations at BB2 station

(0.866±0.062 nmol kg^{-1}). The sharp DFe increase at 1000 m noted at BB1 (1.33±0.14 nmol kg^{-1}) and BB3 (2.00±0.13 nmol kg^{-1}) contrasts with the quickly decreasing concentrations observed at the central BB2 station in Baffin Bay Deep Waters (BBDW) from approximately 1000 to 2300 m (0.962±0.002 to 0.647±0.094 nmol kg^{-1}, respectively; Fig. 7). Dissolved Mn concentrations decreased below AW, remaining nearly uniform across the WIGW, with higher values at stations BB3 and BB1 (0.521±0.011 and 0.600±0.036 nmol kg^{-1}, respectively), and increased concentrations towards the seafloor (4.20±0.008 and 0.768±0.057 nmol kg^{-1}, respectively). Otherwise, at the central BB2 station the DMn in the WGIW was lower (0.416±0.005 nmol kg^{-1}) than over the Baffin Bay slope (BB3 and BB1), noticeably decreasing in BBDW (0.254±0.016 nmol kg^{-1}). As observed at BB3, a sudden increase of DMn occurred in the near-bottom waters (0.736±0.048 nmol kg^{-1}); an increase not observed for DFe (Fig. 7).

The Labrador Sea. Below subsurface waters (>300 m; σ_θ>27.71), DFe continued to increase with depth, across the LSW-2015, ISW and LSW-87/94 water masses, reaching the highest concentrations measured in the Labrador Sea at ~ 2000 m (0.818±0.009 nmol kg^{-1}; σ_θ= 27.82) at the interface between the old LSW-87/94 and the NEADW. Underneath LSW-87/94, DFe concentrations declined across the NEADW, reaching uniformly low concentrations in the deep DSOW (0.677±0.023 nmol kg^{-1}). The vertical distribution of DMn in deep waters, opposite to DFe, generally decreased with depth, with considerably higher concentrations observed across LSW-15 (~400-1000 m; σ_θ= 27.71-27.74) at K1 (0.665 to 0.528 nmol kg^{-1}) compared with LS2 (0.519 to 0.479 nmol kg^{-1}). Underneath LSW-15, no significant concentration differences were observed between LS2 and K1, where concentrations steadily decreased with depth reaching the lowest values (0.306-0.330 nmol kg^{-1}) in the lower boundary of NEADW (~2500 m; σ_θ= 27.86). In the bottom DSOW waters DMn concentrations were moderately higher (0.359-0.385 nmol kg^{-1}) than NEADW (Fig. 7).

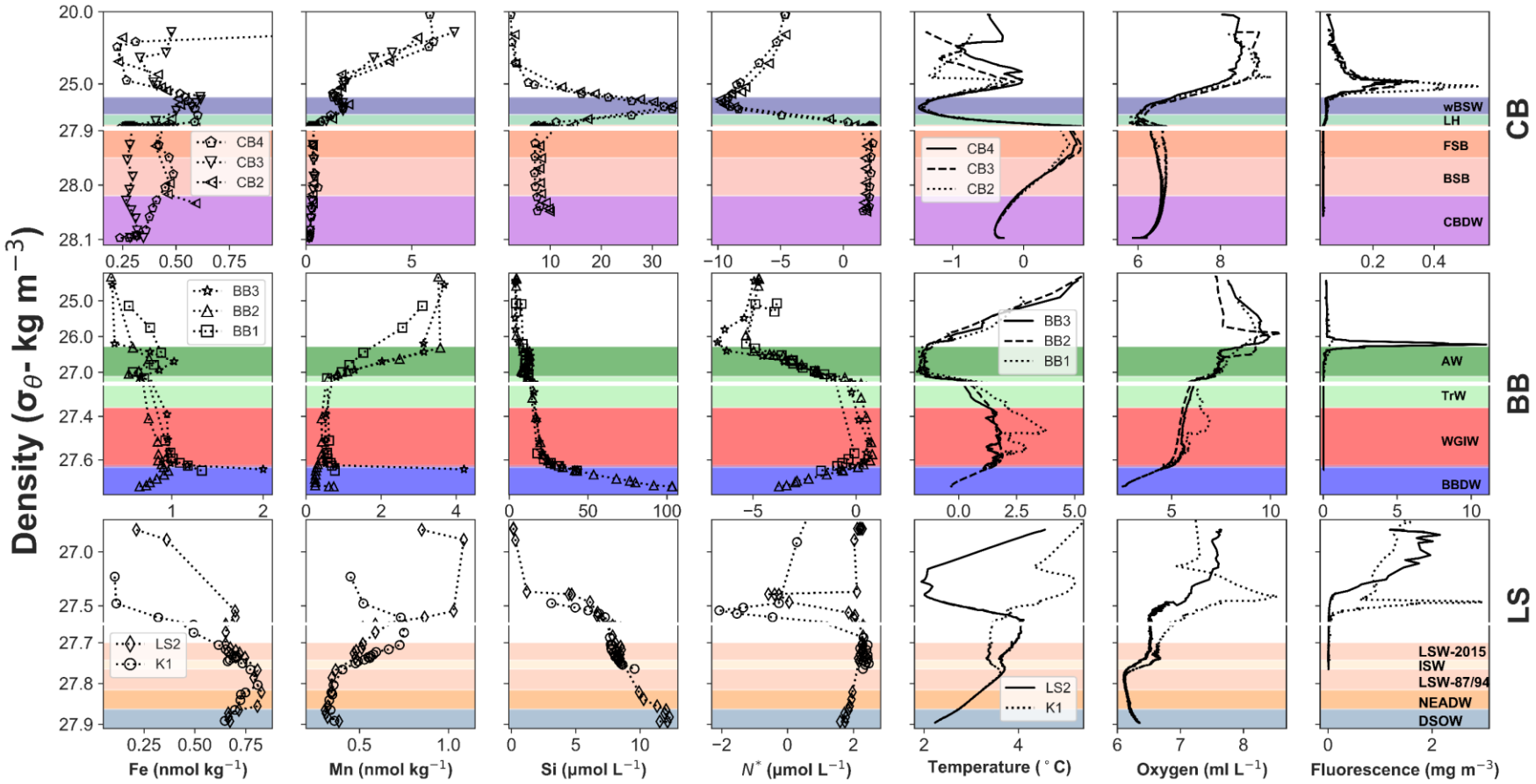

Fig. 7. Profiles of Fe, Mn, Si, N*, Temperature, Oxygen and Fluorescence versus density (σ_θ) for the deep stations in the Canada Basin (upper panel: CB2-CB4), Baffin Bay (middle panel: BB1-BB3) and the Labrador Sea (lower panel: LS2 and K1). N* was calculated from the following equation: N*= ([NO_3^- + NO_2^- + NH_4^+] – 16PO_4^{3-} + 2.9) x 0.87; Gruber and Sarmiento (1997). Silicate and N* data from the Canadian GEOTRACES cruise were provided by ArcticNet (Jean-Eric Tremblay's group). Note the surface water concentration of DFe for the station CB4 in the Canada Basin was extremely high (3.42±0.19 nmol kg^{-1}), and is not displayed in the Figure to emphasize deep water features. Important water masses were superimposed in the plots to facilitate the interpretations and discussion of the trace metal data following Aksenov et al. (2011), Kondo et al. (2016), Tang et al. (2004), Curry et al. (2011), Yashayaev and Loder (2009 and 2016). wBSW: winter Bering Sea Water, LH: Lower Halocline, FSB: Fram Strait Branch, BSB: Barents Sea Branch, CBDW: Canada Basin Deep Water, WGIW: West Greenland Intermediate Water, TrW: transitional water, AW: Arctic Water, BBDW: Baffin Bay Deep Water, LSW: Labrador Sea Water, ISW: Icelandic Slope Water, NEADW: Northeast Atlantic Deep Water, DSOW: Denmark Strait Overflow Water.

5 Discussion

5.1 Dissolved Fe and Mn in surface waters: The role of fresh water inputs and phytoplankton uptake

The relatively high surface concentrations of DMn (3.20-7.02 nmol kg^{-1}) along with DFe (0.225-0.479 and 3.42 nmol kg^{-1} for the PML at CB4) in the Canada Basin agree with previous measurements (Mn: 3.44-6.74 and Fe: 0.2-0.85 nmol kg^{-1}) made in the area (Nakayama et al., 2011; Aguilar-Islas et al., 2013; Kondo et al., 2016; Sim, 2018). Although there are no previous measurements in the CAA, the high DMn and DFe surface concentrations (4.33-10.78 and 0.401-1.91 nmol kg^{-1}, respectively) in this region are in the range of those reported for the Canada Basin shelf break (Mn: 5.48-8.36 and Fe: 0.44-1.66 nmol kg^{-1}) and the Chukchi Sea (Mn: 1.62-13.8 and Fe: 1.11-22.2 nmol kg^{-1}). These regions are both characterized by shallow shelves and elevated riverine freshwater input (Cid et al., 2012; Kondo et al., 2016; Sim, 2018; Vieira et al., 2019). As noted in section 4.1, DMn and DFe decrease dramatically towards Baffin Bay (2.56-3.68 and 0.336-0.763 nmol kg^{-1}, respectively) and the Labrador Sea (0.450-1.09 and 0.106-0.362 nmol kg^{-1}, respectively) toward values that are similar to those reported for surface waters in the North Subarctic Atlantic (Mn: 0.25-0.50 and Fe: 0.02-0.53 nmol kg^{-1}; Measures et al., 2008; Achterberg et al., 2018). In order to identify the sources of Mn and Fe to surface waters (<40 m) in the Canadian Arctic Ocean, we examine the distribution and relationship of these metals in comparison to other physicochemical properties.

As observed in previous studies in the Arctic Ocean, there is a negative correlation between DMn and DFe (to a lesser extent) with salinity (Middag et al., 2011b; Nakayama et al., 2011; Klunder et al., 2012a; Nishimura et al., 2012; Aguilar-Islas et al., 2013; Kadko et al., 2018; Sim, 2018). The highest DMn concentrations are seen in the low salinity range (<31), illustrating the prevailing role of freshwater inputs on the distribution of DMn, as well as DFe in the Canadian Arctic Ocean. Dissolved Mn behaves almost conservatively, exhibiting: 1) a strong negative linear correlation of DMn versus salinity in

Canada Basin (CB2 to CB4), Baffin Bay and Labrador Sea surface waters (R^2= 0.83 and *p-value*< 0.01), with concentrations spanning from 0.450 nmol kg^{-1} in the Labrador Sea to 7.02 nmol kg^{-1} in the Canada Basin, Fig. 8a. 2) a moderate correlation (R^2= 0.55 and *p-value*< 0.01) is found in CAA surface waters (including CB1). This correlation is much stronger if the CAA6 surface data point, which groups more closely with the Canada Basin samples, is excluded from the analysis (R^2= 0.74 and *p-value*< 0.01; Fig. 8a). These different trends are most likely attributable to distance from riverine sources; the CAA is a shallow (~300 m), shelf-dominated region highly influenced by freshwater runoff, glacial meltwater and sediment-seawater interactions (Lammers et al., 2001; Michel et al., 2015; Alkire et al., 2017; Colombo et al., 2019a), which explains the elevated DMn of this region (4.33-10.78 nmol kg^{-1}) and the steeper slope of the linear regression for CAA surface samples (Figs. 6 and 8a). At CAA2, the DMn concentrations (3.72±0.21 nmol kg^{-1}), as well as DFe (0.457±0.066), were slightly lower than the other stations in the archipelago, reflecting the recirculation of Baffin waters with lower DFe and DMn concentrations in northern Lancaster Sound (Wang et al., 2012; Fig. 6). Although we did not analyze the relative contribution of meteoric water and sea ice meltwater to the "freshwater" pool in surface waters (e.g. optimum multiparameter analysis), some inference can be drawn by estimating the concentration of DMn at zero salinity, extrapolated from the CAA regression line (Fig. 8a) assuming conservative behavior, and comparing it with riverine and sea ice meltwater end-members. The projected DMn end-member from the regression line is approximately 45 nmol kg^{-1}, which is substantially higher than the concentrations reported for sea ice and sea ice melt ponds (3-24 nM) in the Arctic Ocean (Campbell and Yeats, 1982; Marsay et al., 2018a). While it is possible that landfast or grounded ice could have higher trace metal concentrations, meltwater is not likely to be the main freshwater input of DMn and DFe to the shelf-dominated CAA region. On the other hand, the projected DMn from CAA surface data is generally lower than the concentrations measured in remote continental rivers (11-54 nM, up to 750 nM during the spring peak discharge) and glacial meltwater (164 nM; Colombo et al., 2019a) in the Canadian Arctic Archipelago. Allowing for non-linear losses in estuaries, riverine inputs are presumably the main contributor to high DMn in CAA surface waters.

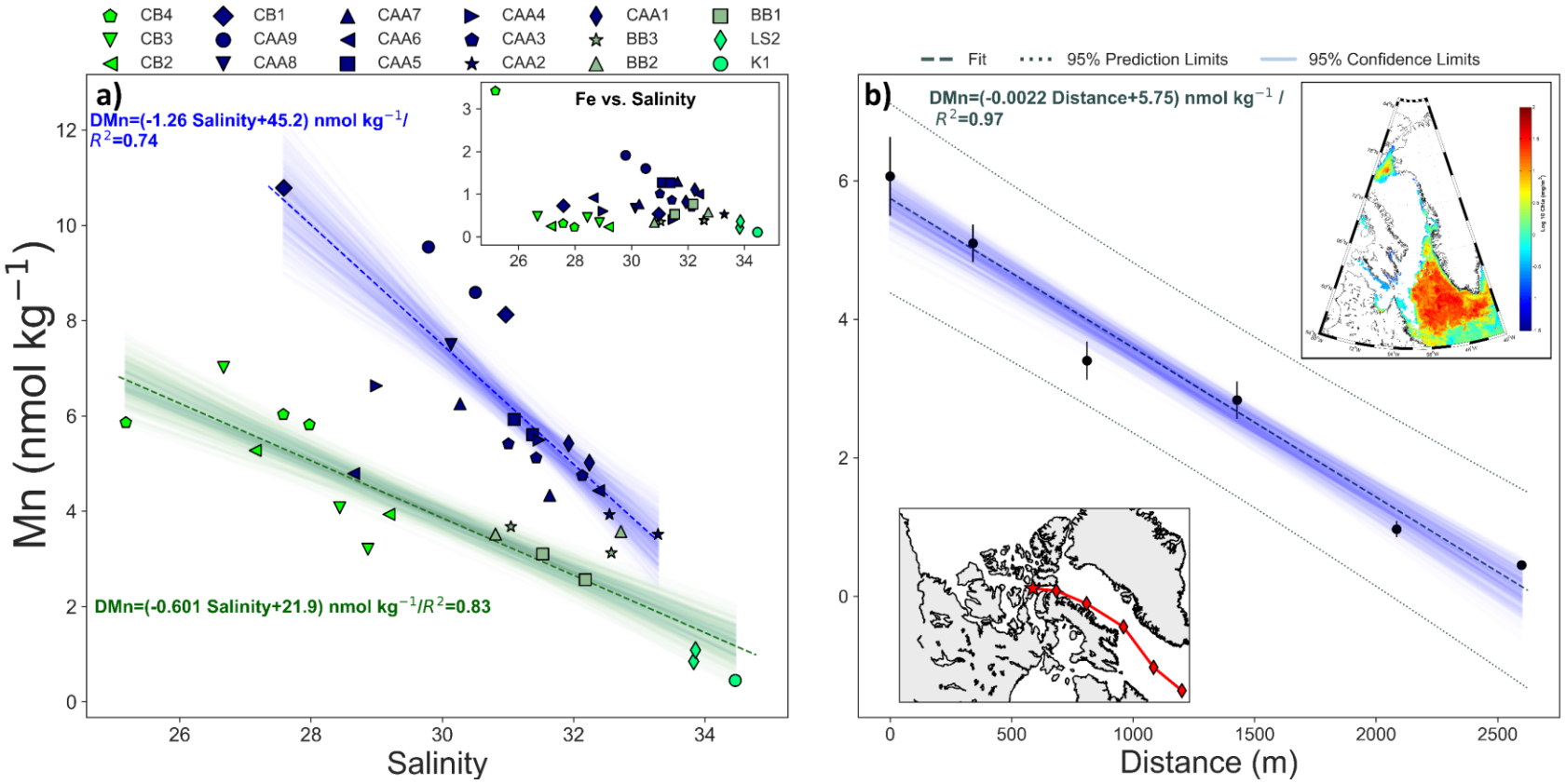

Fig. 8. a) Dissolved Mn concentrations versus practical salinity in the upper 40 m for all the stations. Linear regression lines for the Canada Basin (CB2 to CB4), Baffin Bay and Labrador Sea surface waters (green) and CAA surface waters (blue) are superimposed in the figure. The 95% confidence intervals, estimated by bootstrap resampling of residuals (n=500), are also superimposed in the figure. The density of overlapping lines indicates increased confidence. The inset displays the Fe versus salinity for the same stations. b) Dissolved Mn concentrations (upper 40 m) versus distance from southern Lancaster Sound (CAA4 and CAA3), Baffin Bay coast (BB3), the Davis Strait (BB1) to the Labrador Sea (LS2 and K1), tracing the evolution of DMn in the Arctic outflow from southern Lancaster Sound to the Labrador Sea. Stations included in this plot are displayed in the map and the beginning of the transect is indicated by the red star. The inset shows the monthly-averaged log 10 Chl a concentration in the Labrador Sea (May 2015; data retrieved from MODIS-Aqua sensor: https://oceancolor.gsfc.nasa.gov/l3/), illustrating the intense phytoplankton bloom that took place approximately two months before the sampling. Monthly-averages from 2015, including the entire study area, are presented in Fig. EA5.

The stations in the Canada Basin, Baffin Bay and the Labrador Sea, in contrast to the CAA, are much deeper (~1000-3500 m) and less influenced by continental shelves. Among the deep stations, those in the Canada Basin (CB2 to CB4) had the lowest surface salinity values (25.1-29.2) and the highest DMn concentrations (3.20-7.02 nmol kg^{-1}) compared with Baffin Bay and the Labrador Sea (S: 30.8-34.5; DMn: 0.450-3.68 nmol kg^{-1}). This is the result of the entrainment and accumulation of freshwater and sea ice melt by the Beaufort Gyre, and the influence of relatively fresh Pacific derived waters (Guay et al., 2009; Proshutinsky et al., 2009; Lansard et al., 2012; Kondo et al., 2016; Vieira et al., 2019). The progressive loss of DMn from southern Lancaster Sound (CAA4: 6.07±0.57 and CAA3: 5.10±0.27 nmol kg^{-1}) towards central Baffin Bay (BB2 and BB3: 3.48±0.21 nmol kg^{-1}), Davis Strait (BB1: 2.83±0.27 nmol kg^{-1}) and the Labrador Sea (LS2: 0.97±0.12 and K1: 0.450±0.019 nmol kg^{-1}) may reflect less freshwater inputs from the CAA and adjacent shelves areas with distance along the flow path (Figs. 6 and 8b).

Sinks for DMn and DFe may also be enhanced by phytoplankton uptake, aggregation and sinking in the productive Labrador Sea waters, where the lowest concentrations of these trace elements are measured (Fig. 6). Unlike the other stations sampled in this study, and typical surface DMn data reported from most other basins (Statham et al., 1998; Boyle et al., 2005; Wu et al., 2014; Hulten et al., 2017), surface concentrations in the Labrador Sea are lower than subsurface samples and does not show a DMn surface maximum (Figs. 3b, 5 and 6). Similar profiles have been found in the Weddell Basin, where the near depletion of DMn in surface waters was attributed to fast biological Mn uptake under Fe limiting conditions - due to enhanced oxidative stress in Fe-limited phytoplankton and the resulting expression of Mn-containing superoxide dismutases - coupled with the lack of external Mn sources (Middag et al., 2011a; Middag et al., 2013). Intense phytoplankton spring blooms, triggered by increased irradiance and mixed-layer shoaling, occur in the Labrador Sea (Frajka-Williams et al., 2010). These Labrador Sea blooms are the most intense in the Canadian Arctic Ocean, typically peaking in May and slowly decreasing in intensity throughout the summer. When samples were collected in the Labrador Sea (July,

2015), an intense bloom had recently been observed (May, 2015; Figs. 8b and EA5); this bloom was one of the largest in recent years (https://oceancolor.gsfc.nasa.gov/l3/). Iron-limiting conditions have not been documented to date in the Labrador Sea, mainly due to a paucity of DFe data. However, studies nearby have shown that surface waters of the Iceland and Irminger basins experience seasonal Fe-limiting conditions coincident with the spring bloom, when relatively high macronutrient concentrations were still found in surface waters (Nielsdóttir et al., 2009; Ryan-Keogh et al., 2013; Achterberg et al., 2018). As a first approximation, to evaluate whether phytoplankton in Labrador surface waters (<40 m) were potentially limited by Fe relative to PO_4^{-3}, we calculated the Fe* index (Fe*= DFe – 0.47[PO_4^{-3}]) developed by Parekh et al. (2005). Positive Fe* values indicate that DFe is sufficiently high to allow full utilization of PO_4^{-3}, while negative values suggest potential DFe deficiency. At station K1 (the farthest from Davis Strait) surface Fe* was close to 0 (0.009) whereas at LS2 station the values were slightly higher (0.196-0.330). Although no negative values were observed in this study, the low Fe* at K1 suggests potential Fe stress and the possibility that Fe availability might limit phytoplankton yield in the Labrador Sea. However, the macronutrient concentrations in Labrador Sea surface waters were extremely low at the time of our sampling (post bloom) arguing against acute, severe Fe-limitation of nutrient uptake there. This contrasts with observations of incomplete nitrate drawdown attributed to Fe-limitation in the high latitude North Atlantic in surface waters of the Iceland and Irminger Basins (Ryan-Keogh et al., 2013). It should be noted that Fe stress conditions in surface waters are not anticipated to be alleviated during winter mixing in the Labrador Sea as nutricline waters are likely to be Fe-depleted relative to phytoplankton metal-macronutrient demand, with Fe* values ranging from -0.08 to 0.03 and NO_3^-/DFe ratios (29338-31079) at K1 well above the 15000:1 ratio which allow the complete consumption of NO_3^- (Kaupp et al., 2011). Therefore, increased biological uptake of DMn and DFe coupled with limited freshwater inputs of these metals are likely to explain their low Fe concentrations and DMn minimum in Labrador Sea surface waters. These findings highlight the need for a more comprehensive study of Fe-phytoplankton interactions during the spring-summer season that includes bioassay/incubation

experiments and measurements of cellular Fe-stress indicators to unequivocally ascertain whether Fe limitation of primary production is important in the Labrador Sea.

The main sources of DFe to surface waters in the Canadian Arctic Ocean are expected to be similar to those of DMn. However, the distribution of DFe deviates from the trends observed for DMn in surface waters, which reflect its unique aqueous biogeochemistry. Dissolved Fe is less soluble, more scarce relative to its biological requirement for microbes, and has faster oxidation and complexation kinetics than Mn (Landing and Bruland, 1987; Bruland et al., 1991; Nico et al., 2002; Hansard et al., 2009; Mendez et al., 2010; Aguilar-Islas et al., 2013; Morel et al., 2013; Gerringa et al., 2015; Buck et al., 2018). Surface DFe concentrations in the Labrador Sea, Baffin Bay and most of the stations in CAA generally increase with decreasing salinity, but deviations from this relationship (lower DFe than predicted by surface salinity) are evident in the Canada Basin and CAA4, 6 and CAA8 stations.

5.2 Dissolved Fe and Mn in shelf seas and subsurface waters: Shelf-ocean interactions, scavenging removal and advective transport

5.2.1 Influence of Chukchi Sea derived waters on the Fe and Mn signature in subsurface waters in the Canada Basin

Noteworthy subsurface maxima of DFe (0.541±0.060 nmol kg^{-1}) and DMn (1.37±0.41 nmol kg^{-1}) were observed in the wBSW within a narrow depth range (100–300 m) across the Canada Basin (Figs. 3 and 7). The highest concentrations coincided with a peak in major algal nutrient concentrations (Si: 34, PO_4^{-3}: 1.8 and NO_3^-: 16 µmol L^{-1}), and minima in N^*, temperature and oxygen values (-10, -1.5 °C and 6 mL L^{-1}, respectively) at a density of $\sigma_\theta = 26.5$ (Fig. 7). This characteristic wBSW signature is imprinted during its flow across the shallow and highly productive Chukchi Sea, where intense organic matter remineralization on the seafloor promotes sedimentary denitrification/anammox, leading to negative N^* values, and increasing the benthic flux of reduced species of Fe and Mn to the overlying wBSW as sediment porewater O_2 and redox potential diminishes (Chang and Devol, 2009; Kondo et al., 2016;

Granger et al., 2018; Vieira et al., 2019). Similar subsurface peaks (σ_θ = 26.5) of DFe and DMn, along with a nutrient maximum and low N^* values, were observed along the Chukchi slope (Fe: 4.53±1.01 and Mn: 37.7±18.3 nM) and the Canada Basin (Fe: 1.62±0.41 and Mn: 1.34±0.57 nM), with the metal concentrations decreasing exponentially with distance from the shelf break (Hioki et al., 2014; Kondo et al., 2016).

It is not surprising that DFe concentrations in the wBSW reported by Hioki et al. (2014) and Kondo et al. (2016) were higher than those measured in this study (D5 station: 1.62±0.41 nM versus CB2-CB4 stations: 0.541±0.060 nmol kg^{-1}), since their D5 station was located ~ 350 km from Chukchi shelf while CB2-CB4 stations were located more than 600 km away from the shelf. Nonetheless, DMn concentrations measured at D5 (1.34±0.57 nM) were comparable to those measured in this study (1.37±0.41 nmol kg^{-1}). This divergent behavior of DFe and DMn could be attributed to the more rapid oxidation kinetics and enhanced scavenging loss of Fe relative to Mn, that without organic ligand stabilization, Fe is rapidly removed from the water column (Sunda et al., 1983; Field and Sherrell, 2000; Thuróczy et al., 2011; Wu et al., 2011; Klunder et al., 2012b; Buck et al., 2018).

5.2.2 Benthic sources of dissolved Fe and Mn in the shallow Canadian Arctic Archipelago environment

The concentrations of Fe and Mn measured in the Canadian Arctic Archipelago (CAA) were the highest observed in this study (Figs. 3, 4 and 5), with subsurface concentrations comparable to those found in other shallow shelf regions in the Arctic Ocean such as the Chukchi Sea (Fe: ~3-15 nM) and the Laptev and Barents shelves (Fe: ~2-12 and Mn: ~3-5 nM), albeit DMn concentrations in Chukchi near-bottom waters were considerably higher (~10-81 nM) than in the CAA (Middag et al., 2011b; Klunder et al., 2012a; Kondo et al., 2016; Vieira et al., 2019).

Below the surface, the most striking feature in the distributions of dissolved Fe and Mn is the spatial variability observed between the western and the eastern CAA, with significantly lower concentrations

548 and no evidence of benthic inputs of these trace metals in M'Clure Strait (CB1) and Viscount Melville
549 Sound (CAA8) compared with the stations located in the eastern Parry Channel (CAA1-CAA7; Figs. 3, 4,
550 5 and 9a). This discrepancy is attributed to the advection of Arctic waters with low Fe and Mn from the
551 Canada Basin, less mixing in the western CAA, and enhanced sedimentary Fe and Mn inputs in the
552 eastern CAA. Subsurface Arctic waters (wBSW and LH), advected from the Canada Basin, carry
553 relatively low DFe and DMn (0.488±0.097 and 1.31±0.52 nmol kg^{-1}) to western Parry Channel (~500 m)
554 up to Barrow Strait, where the sill depth (~120 m) restricts the continued direct flow downstream (Wang
555 et al., 2012; Colombo et al., 2019b). Mixing is intense throughout the shallow CAA as result of tidal
556 forcing, shear instabilities and the breaking of internal waves over the rough topography in the small
557 straits and conduits forming the archipelago (Hannah et al., 2009; Hughes et al., 2017; Hughes et al.,
558 2018). However, mixing is particularly strong in the central sills area (~120 m) near Barrow Strait
559 (confined by Bathurst, Cornwallis, Devon, Sommerset and Prince of Wales Islands) and in Penny Strait
560 (Fig. 9a), where averaged diapycnal diffusivities and buoyancy fluxes are up to an order of magnitude
561 larger than in the western CAA (Hughes et al., 2017). As expected, the Arctic outflow is greatly modified
562 over the shallow Barrow Strait area and in Lancaster Sound by incorporating river and glacial runoff,
563 mixing with Baffin Bay waters, and most importantly, by interacting with bottom topography (Wang et
564 al., 2012; Hughes et al., 2017; Colombo et al., 2019b; Colombo et al., 2019a). In this context, the elevated
565 DFe and DMn measured in subsurface waters and the sharp rise in their concentration towards near-
566 bottom waters in eastern Parry Channel stations (CAA1-CAA7) are likely associated with sedimentary
567 inputs.

568 The release of Fe and Mn from sediments is identified as a key source that explains the elevated
569 concentrations of these metals in shelf-slope regions worldwide (Johnson et al., 1999; Lam and Bishop,
570 2008; Cullen et al., 2009; Klunder et al., 2012a; Hatta et al., 2015; Milne et al., 2017; Cheize et al., 2019;
571 Vieira et al., 2019). Although the release of Fe and Mn from anoxic sediments (reductive dissolution)
572 cannot be neglected (Klar et al., 2017), it is not considered to be the primary mechanism taking place in

573 the CAA. All studied CAA stations were well oxygenated, including the bottom waters which had oxygen
574 concentrations above 200 µmol kg^{-1} (4.6 ml L^{-1}) and N^* values ranging from -6.3 to 2.5. Under the strong
575 reducing sediment conditions present in the highly productive Chukchi shelves, near-bottom waters had
576 much lower N* values (~ -15) and much higher DMn concentrations (~10-81 nM) than observed in the
577 CAA (Hioki et al., 2014; Kondo et al., 2016; Vieira et al., 2019). This suggests stronger benthic reductive
578 inputs in the Chukchi Sea region compared to the CAA. Likewise, the release of nutrient-like trace metals
579 during the remineralization of organic matter does not appear to be a main source in the CAA, given the
580 poor relationship between DFe and apparent oxygen utilization (R^2= 0.03 and *p-value*= 0.11). Thus, the
581 rise of DFe and DMn from 130 m toward the seafloor along the eastern Parry Channel is likely related to
582 the resuspension, desorption and/or dissolution from sediment particles during mixing, as indicated by the
583 moderate (R^2= 0.52 and *p-value*< 0.001) and strong (R^2= 0.67 and *p-value*< 0.001) negative correlations
584 found between DFe and DMn versus transmissivity (lower transmissivity values indicate greater
585 suspended particle matter concentrations; Figs. 9b and 9c). Other factors such as the distance from the
586 deepest sample to bottom sediments do not explain the variability in metal concentrations observed in
587 near-bottom waters. The distance from the deepest samples to the seafloor for the stations sampled in
588 western CAA (CB1 and CAA8), which do not show any Fe and Mn enrichment in near-bottom waters,
589 was 61 and 113 m; however, the stations CAA1 and CAA3, located in eastern Parry Channel at a
590 comparable distance from the seafloor (72 and 98 m, respectively), do show a clear enrichment of these
591 trace metals (Fig. 9a). Moreover, in eastern CAA, bottom inputs of DFe and DMn can be traced not only
592 at the deepest samples, but also in overlying samples. The distributions of particulate Fe and Mn from the
593 same CAA stations show similar trends (Li, 2017), with a sharp increase in near-bottom waters for those
594 stations located in Barrow Strait and Lancaster Sound (CAA1-CAA7), with relatively low concentrations
595 found in the western CAA (CB1 and CAA8), further supporting the importance of sediment resuspension
596 and benthic inputs of both dissolved and particulate Fe and Mn in eastern Parry Channel.

The consistently higher concentrations of both DFe and DMn measured in the stations located along the northern edge of Parry Channel relative to the southern ones are potentially explained by increased sediment resuspension due to the recirculation of Baffin Waters in this region (Fig. 9a). Additionally, the presence of extensive glaciers distributed along the western sides of Ellesmere, Devon and Baffin islands may be a source of more easily reducible Fe oxides and soluble Fe^{+2} containing minerals compared to sediments close to the ice-free coast of southern Parry Channel (Lenaerts et al., 2013; Henkel et al., 2018). Lastly, the significantly (*p-value*< 0.01) lower subsurface DFe and DMn concentrations present at station CAA2 compared to CAA1 (Fig. 9a), despite their close proximity (~20 km apart), are related to the different water masses affecting these stations. Station CAA1, as well as CAA5 and CAA6, are located in close proximity to the Devon Island coast (~ 5km; Fig. 9a), receiving inputs of glacial runoff which are recognized to have extremely high concentrations of DFe and DMn (212 and 164 nM; Colombo et al., 2019a). Conversely, the station CAA2 is influenced by the recirculation of low DFe and DMn Baffin waters; these differences can be detected in the temperature and salinity profiles, with CAA1 waters noticeable fresher and colder than at CAA2 (Fig. 2b), and from the distributions of dissolved lead (Colombo et al., 2019b).

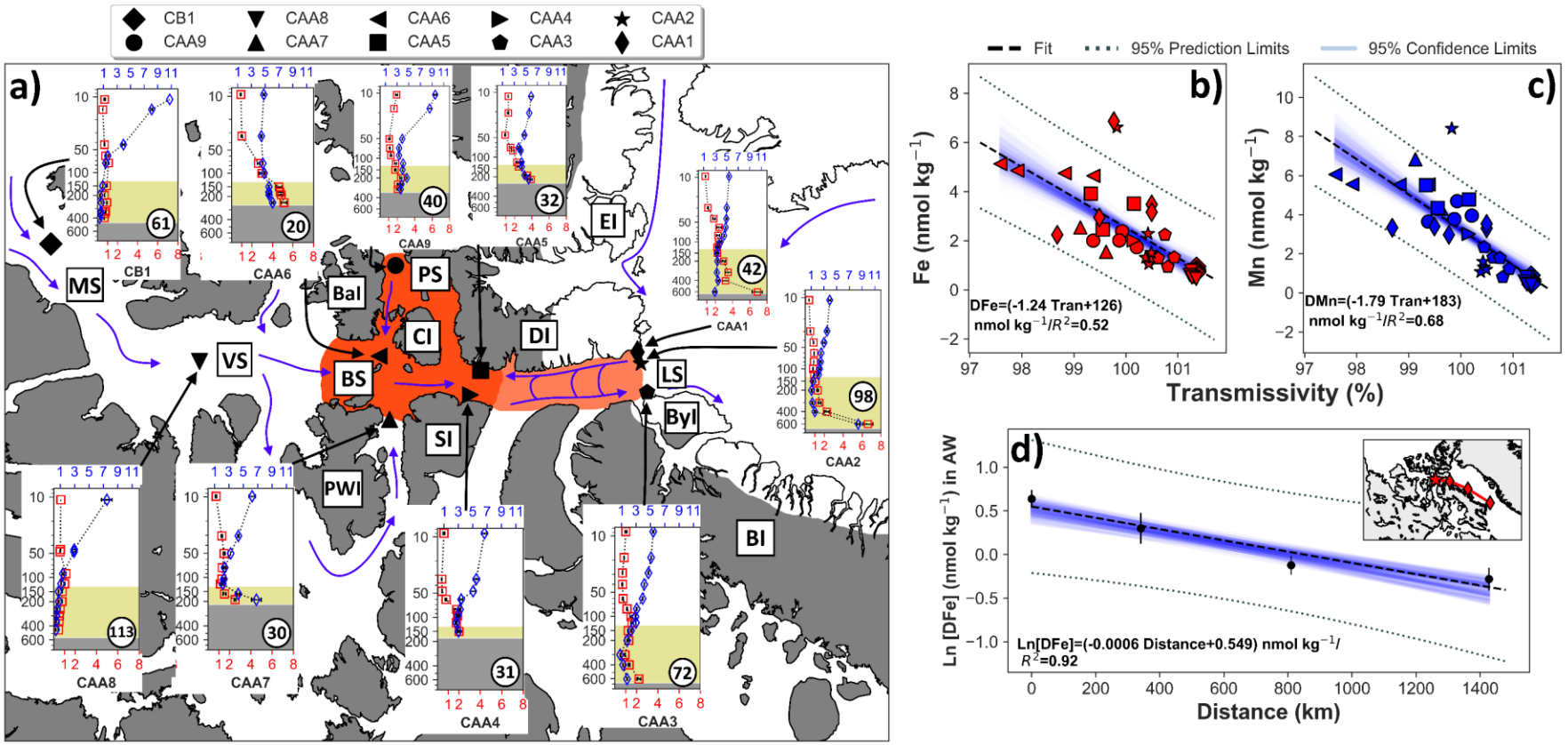

Fig. 9. a) Sampled stations and circulation pathways (blue arrows) in the CAA (after Michel et al., 2006; Wang et al., 2012); red and light red shaded area: conceptual scheme displaying intense diapycnal and tidal mixing in Barrow Strait area and eastern CAA (modified from Hannah et al., 2009; Hughes et al., 2017; Hughes et al., 2018). Dissolved Fe (red profiles) and Mn (blue profiles) concentrations (nmol kg^{-1}) for each CAA station are superimposed in the Figure panel 8a; the gray shading indicates the seafloor, the pale green shaded area indicates those samples below 130 m, and the number within a white circle is the distance (m) from the deepest sample to bottom sediments. MS: M'Clure Strait, VS: Viscount Melville Sound, BS: Barrow Strait, PS: Penny Strait, LS: Lancaster Sound, BaI: Bathurst Island, CI: Cornwallis Island, SI: Somerset Island, PWI: Prince of Wales Island, DI: Devon Island, ByI: Bylot Island, EI: Ellesmere Island, BI: Baffin Island. Parry Channel is the main pathway in central CAA connecting M'Clure Strait with Lancaster Sound. b) and c) Dissolved Fe (red symbols) and Mn (blue symbols) versus transmissivity for CAA samples below 130 m (values greater than 100% indicate offset in the calibration). Linear regression lines and R^2 values are displayed in the Figure, as well as the 95% prediction limits and the 95% confidence intervals, estimated by bootstrap resampling of residuals (n=500). The density of overlapping lines indicates increased confidence. d) Natural logarithm of dissolved Fe concentrations in the Arctic Waters (AW; σ_θ= 26.28-27.12) versus distance from southern Lancaster Sound (CAA4 and CAA3), Baffin Bay coast (BB3) to the Davis Strait (BB1), showing an exponential decrease in DFe concentrations (*DFe= 1.732 $e^{-0.0006 \text{ Distance}}$ or Ln [DFe]= -0.0006 Distance+0.549 when it is linearized*). Stations included in this plot are displayed in the inset map and the beginning of the transect is indicated by the red star and the linear regression line, R^2 value and the 95% prediction limits and the 95% confidence intervals are displayed in the figure.

5.2.3 The importance of CAA waters modulating subsurface DFe and DMn in Baffin Bay and the Labrador Sea

The CAA is an important pathway linking the Canada Basin with Baffin Bay, whereby Arctic derived waters are exported to the North Atlantic (Jones, 2003; Beszczynska-Möller et al., 2011). In Baffin Bay this Arctic outflow is mixed with the WGC evolving into the fresher (S=32.0-33.7) and colder (T< 0 °C) Arctic Water (AW; Fig. 2c). During its flow through the shallow CAA shelves, Arctic derived waters are enriched in Fe (section 5.2.2), relative to Canada Basin concentrations, advecting this high signature to the Baffin Bay interior, where a DFe peak (0.753-1.025 nmol kg^{-1}) is observed in subsurface AW (Figs. 3a and 7). Dissolved Fe concentrations in AW (BB3>BB1>BB2) reflect the proportional contribution of Arctic derived waters, where BB3 is most influenced by this outflow followed by BB1 (~85 and ~60%), while BB2 station, located in the center of the bay, is more isolated from the fresh, cold and Fe rich coastal CAA outflow (~40%; Colombo et al., 2019b). The offshore transport of this AW DFe-rich plume along isopycnal surfaces (σ_θ= 26.28-27.12) can be followed for more than 1400 km from the western Parry Channel in the CAA (station CAA4) to Davis Strait (station BB1), with the Baffin Current (Fig. 9d), but no traces of this high DFe plume is found in the Labrador Sea (Figs. 3a and 7). An exponential function ($DFe = A\, e^{[-d/Lo]}$, where A: 1.732 nmol kg^{-1}, d: distance from station CAA4 [km] and L_o: scale length of offshore transport, ~1450 km; Fig. 9d) best describes (R^2= 0.92, *p-value*< 0.05) the offshore decrease of DFe from the station CAA4 (Fig. 9d). We estimate the scale length of DFe transport as the distance over which concentrations drop to approximately 37% or 1/e of the initial values (Johnson et al., 1997; Klunder et al., 2012b; Aguilar-Islas et al., 2013). The scale length of offshore transport of DFe in Baffin Bay (L_o= ~1450 km) is 4-5 times greater than those calculated for the Canada and Nansen basins (380 and 260 km), where the currents are predominantly parallel to continental slopes (Klunder et al., 2012b; Aguilar-Islas et al., 2013), and 4 times lower than the scale length of DFe observed from central California coast to the Pacific Ocean at 1000 m depth (5000 km ; Johnson et al., 1997). The increased length scale transport of DFe observed in this study compared to the Canada and Nansen basins

presumably reflect both an increased strength of the horizontal advection of DFe relative to sampled stations, as well as lateral inputs from the Baffin Bay slope. The enhanced biological and abiotic sinks of DFe over the productive, shallow and extensive shelves and slopes in Baffin Bay (<1000 m deep) may explain the more modest advective transport scale length of DFe compared with the transect sampled in the Pacific Ocean (>4000 m deep). Subsurface (40-300 m) waters in the Labrador Sea do not exhibit a DFe peak, but the concentrations increase rapidly with depth and their vertical distributions are primarily controlled by remineralization rather than by continental advective fluxes, as suggested by the sharp increase in nutrient concentrations (Fig. 7) and the very strong positive correlation between DFe and Apparent Oxygen Utilization (AOU; R^2= 0.92, *p-value*< 0.001, n=8) in these waters. We expand upon the relationship of DFe and AOU and the importance of remineralization in controlling DFe distributions in section 5.3.1.

Dissolved Mn concentration in subsurface Baffin Bay waters (40-300 m) sharply decreases with depth till 300 m (σ_θ= 27.39; Fig. 7), and its distribution appears to be largely controlled by particle scavenging and oxidative removal of Mn^{+2} below the surface waters (Landing and Bruland, 1980; Sunda and Huntsman, 1994; Statham et al., 1998). The AW peak in DMn concentrations is believed to be obscured in Baffin Bay due to the elevated surface and subsurface concentrations measured in this basin. However, the DFe/DMn ratio of AW (0.610±0.058) is clearly distinguished from overlaying (0.281±0.027) and underlying (1.06±0.18) waters, and is similar to the ratio found in CAA3-4 (0.606±0.076) in the same density range. The subsurface DMn concentrations in Baffin Bay are higher than those measured in the Labrador Sea (1.24±0.78 vs. 0.735±0.148 nmol kg^{-1}; Figs. 3b and 7). This could be explained by the differences in surface DMn concentrations between Baffin Bay (influenced by freshwater inputs) and the Labrador Sea (3.26±0.38 vs. 0.795±0.263 nmol kg^{-1}), and the AW outflow in Baffin Bay advecting high DMn from the CAA.

5.3 The contrasting biogeochemistry of DFe and DMn in deep waters

5.3.1 Dynamic interplay of DFe inputs versus scavenging removal in deep waters

Dissolved Fe concentrations below 300 m in the Canada Basin are the lowest among the deep stations sampled in this study, and their distributions, contrary to what is observed in Baffin Bay and the Labrador Sea, are not easily explained by remineralization processes. We estimate the influence of remineralization of sinking organic particles on the deep water DFe distributions, using the relationship between apparent oxygen utilization (AOU) and DFe concentrations. The AOU is calculated as the difference between measured dissolved oxygen concentration and its saturation concentration, as result of organic matter respiration; DFe:AOU correlation analyses have been used extensively in the literature, providing insights about inputs of DFe from remineralization of organic matter (Bergquist and Boyle, 2006; Wu et al., 2011; Rijkenberg et al., 2014; Fitzsimmons et al., 2015; Hatta et al., 2015; Pham and Ito, 2018). In the Canada Basin, no significant correlations are found between DFe and oxygen (R^2= 0.10, *p-value*= 0.11, n= 26) or DFe and AOU (R^2= 0.09, *p-value*= 0.13, n= 26) in the deep water column, which suggest that remineralization is not a significant source of DFe. This is not surprising as the Canada Basin has one of the lowest primary productivity levels in the Arctic Ocean, and extremely low vertical fluxes of particulate organic carbon (Hill et al., 2013; Varela et al., 2013; Brown et al., 2014; Crawford et al., 2015; Li, 2017). The vertical distributions of DFe in the AL (~300-1000 m) and the CBDW (>1200 m) are a result of the advection of Atlantic waters travelling in the Arctic Circumpolar Boundary Current (ACBC) and the subsequent scavenging within the CBDW. This was also observed in the Eurasian Basin where the Fe signature in Atlantic-derived waters is reduced due to scavenging along their cyclonic circulation from eastern Nansen Basin to the Makarov Basin (Klunder et al., 2012b).

Below the wBSW, similar DFe distributions were observed at stations CB2 and CB4, where the concentrations in the AL were slightly lower (0.405-0.419 nmol kg^{-1}) in the warm FSB core (~500 m and σ_θ= 27.92) than in the deeper, colder and fresher BSB (~600-1000 m and σ_θ= 28.00; 0.467±0.012 nmol kg^{-1}), with concentrations decreasing with depth in the CBDW (0.409 to

0.238 nmol kg^{-1}). In contrast, the distribution of DFe at CB3 appears different from the other two stations, with relatively uniform and significantly lower concentrations from 300 to 3000 m (0.293±0.017 nmol kg^{-1}; Fig. 7). Dissolved Fe in the AL (FSB + BSB) in the Canada Basin is lower than that measured in the eastern and western Nansen Basin (0.609±0.106 and 0.548±0.071 nmol kg^{-1}) and comparable to the Amundsen (0.420±0.044 nmol kg^{-1}) and the Makarov (0.362±0.066 nmol kg^{-1}) basin concentrations (Klunder et al., 2012b). This difference in the DFe distributions, as well as in particulate Fe and dissolved ^{230}Th (Li, 2017; Grenier et al., 2019), between CB2 and CB4 relative to CB3 is best explained by varying influence of the ACBC. Due to their locations, both CB2 and CB4 are more directly impacted by the cyclonic circulation of the FSB and the BSB (ACBC components) around the basin compared to CB3 (Fig. 1). The ACBC travels along the Siberian, Chukchi Plateau, Alaskan and Canadian continental slopes, where DFe is mobilized from the continental margin (sediment resuspension, reductive dissolution, etc.), entraining high concentrations to the Canada Basin interior (Nakayama et al., 2011; Klunder et al., 2012b; Aguilar-Islas et al., 2013; Kondo et al., 2016). However, as was observed for the wBSW, this high DFe signature is rapidly attenuated before reaching the more central and offshore CB3 station. The higher DFe measured in the BSB compared to FSB waters, reflects the circulation pathways of these water masses. The BSB flows around the rim of the Arctic Ocean in close proximity to the Fe-rich continental margin while the FSB flow diverts toward the deep basin earlier as it enters the Arctic Ocean (Aksenov et al., 2011). In the deep, old and isolated (~200-500 years; Tanhua et al., 2009) CBDW, the losses of DFe by scavenging dominate over remineralization and/or advective inputs, as a continuous decrease of DFe with depth at CB4 is observed (Fig. 7; only the deepest CB3 and CB4 stations capture this water mass). In CBDW a strong linear relationship between DFe concentration and water mass age (Tanhua et al., 2009; Fig. 10b) is found at CB4 ($DFe= [-0.0005\ Age\ + 0.473]\ nmol\ kg^{-1}$; R^2= 0.96 and *p-value*< 0.001; Fig. EA6), where DFe is lost at an approximate rate of 0.5 pmol kg^{-1} $year^{-1}$. However, this relationship is not present at CB3, where uniformly low concentrations were measured from 1000 to 3500 m (0.303±0.024 nmol kg^{-1}), presumably due to isolation of this station from Fe enriched waters advected in the ACBC.

In Baffin Bay and the Labrador Sea, remineralization of sinking particles appears to have a predominant role in shaping the subsurface and deep distribution of DFe in the TrW, WGIW and LSW, while scavenging dominates in the deeper BBDW, NEADW and DSOW. In Baffin Bay from 300 to 1000 m, DFe concentrations show a very strong positive linear correlation with AOU, with distinct trends for BB1 and BB3 stations (*DFe= [(0.0054 AOU) / µmol L^{-1} + 0.463] nmol kg^{-1};* R^2= 0.84 and *p-value*< 0.001; Fig. 10a) and BB2 (*DFe= [(0.0030 AOU) / µmol L^{-1} + 0.498] nmol kg^{-1};* R^2= 0.82 and *p-value*< 0.05; Fig. 10a). The deepest sample at BB3 is excluded from this analysis as it shows a clear sedimentary input evidenced by notably high DFe and DMn (Figs. 3 and 7), and high particulate Fe and Mn (approximately one order of magnitude higher values than overlaying waters; Li, 2017). The difference in the DFe remineralization rates (slope of DFe:AOU plot) and the DFe concentrations between BB1 and BB3 versus BB2 is associated with enhanced scavenging at BB2. In the center of Baffin Bay, BB2 is largely isolated from the cyclonic circulation of WGIW and BC, so that subsurface waters (~300-800 m) have a residence time of greater than four years, unlike BB1 and BB3 where there is a larger proportion of shelf-influenced waters (Colombo et al., 2019b). In the Labrador Sea, DFe and AOU also show a very strong correlation (*DFe= [(0.0055 AOU) / µmol L^{-1} + 0.504] nmol kg^{-1};* R^2= 0.81 and *p-value*< 0.001) from approximately 300 to 2400 m, and the rate of remineralization and pre-formed DFe (slope and intercept of the DFe:AOU plot) are similar to those found at BB1and BB3 (Fig. 10a). Despite the similar DFe:AOU trends, the concentrations are considerably higher in Baffin Bay than in the Labrador Sea (Figs. 3a and 10a). As pre-formed DFe concentrations (other sources of Fe besides remineralization) are virtually the same for both basins (~0.48 nmol kg^{-1}), the higher DFe (0.942±0.151 nmol kg^{-1}), as well as the higher nutrient concentrations, measured in Baffin Bay are believed to be the result of increased remineralization (>AOU) of sinking organic particles from the highly productive surface waters fueled by Pacific-derived nutrients (Varela et al., 2013; Lehmann et al., 2019).

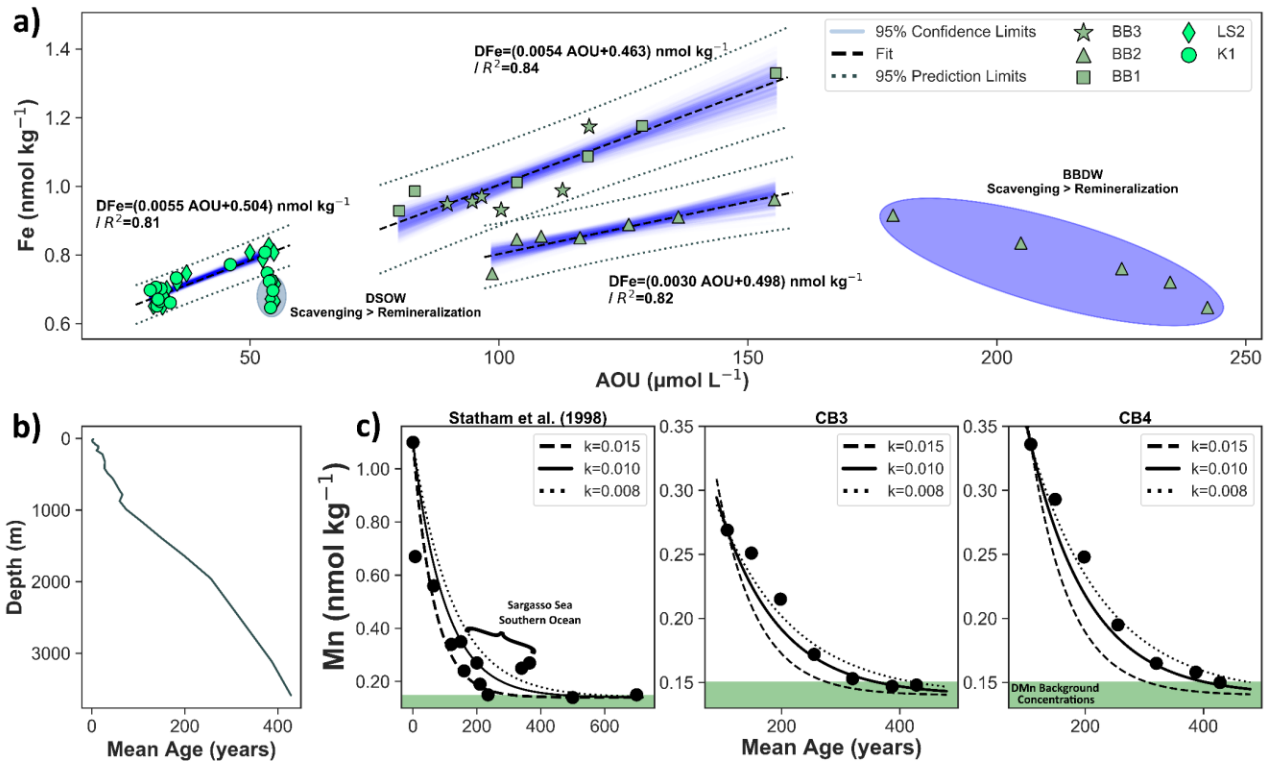

748

749 **Fig. 10.** a) AOU and DFe relationship in deep waters (>300 m) in Baffin Bay and the Labrador Sea. Linear regression lines
750 and R^2 values are displayed in the figure, as well as the 95% prediction limits and the 95% confidence intervals, estimated by
751 bootstrap resampling of residuals (n=500). The density of overlapping lines indicates increased confidence. b) Estimated mean
752 ages for Canada Basin waters from chlorofluorocarbon data (Tanhua et al., 2009); age profiles from the stations 30015
753 (Lat./Lon.: 75.3/-144.2; JOIS97 cruise) and 10008 (Lat./Lon.: 75.5/-150.2; Beringia cruise) were chosen due to their close
754 proximity to our sampled stations. c) DMn versus water mass age, including data from Statham et al. (1998) and from Canada
755 Basin Deep Waters (this study). Pseudo-first order scavenging model solutions, using different scavenging constants, are
756 superimposed in the plots (for details refer to text); the best fit described by Statham et al. (1998) and chosen in this study are
757 displayed with dashed and solid lines, respectively. Green shaded bands indicate background DMn concentrations
758 (0.10-0.15 nmol kg^{-1}) measured in deep ocean waters (for details refer to text).

759

760 The DFe concentrations in Labrador Sea Waters (~300 to 2000 m; LSW-2015 and LSW-87/94)
761 agree with the values reported for the Irminger Basin (Achterberg et al., 2018) and the North Atlantic
762 Subarctic Gyre (NASG) in the GEOTRACES GA02 transect (Rijkenberg et al., 2014; Schlitzer et al.,
763 2018), with the highest concentrations (0.818±0.009 nmol kg^{-1}) observed at approximately 2000 m
764 corresponding to the interface between LSW-87/94 and NEADW. These first measurements in the
765 Labrador Sea support the hypothesis that the LSW is enriched in DFe by continental sediment
766 resuspension during its southward flow along the North American continental slope in the deep western
767 boundary current (Fitzsimmons et al., 2015; Hatta et al., 2015). The concentrations found in LSW at the

offshore stations from Massachusetts to the Bermuda Atlantic Time Series station (line W) are higher (1.1±0.2 nM; Hatta et al., 2015) than those measured in this study (0.716±0.056 nmol kg^{-1}). In the absence of direct measurements of DFe, Hatta et al. (2015) estimated the preformed and regenerated DFe in the Labrador Sea (0.34-0.47 nM), and projected a DFe enrichment of about 55% in LSW as results of continental shelf interactions. Results from this study suggest that the extent of DFe enrichment is smaller (35%) than previously inferred by Hatta et al. (2015), our lack of information from stations closer to the shelf and slope preclude us from being absolute in this assertion. Lastly, we estimate the Fe:C ratios of sinking organic matter in Baffin Bay (8.6 μmol mol^{-1}) and the Labrador Sea (8.8 μmol mol^{-1}) converting AOU to remineralized organic carbon using a AOU:C ratio of 1.6 (Martin et al., 1987). Our estimated Fe:C ratios are similar to those reported for the Iceland Basin (12.1 μmol mol^{-1}; Achterberg et al., 2018) and for the subtropical North Atlantic Ocean (7.1-12.8 μmol mol^{-1}; Sunda, 1997; Bergquist and Boyle, 2006; Fitzsimmons et al., 2013), and slightly higher than estimates for Line W (5.69 μmol mol^{-1}; Fitzsimmons et al., 2015). However, the inferred Fe:C ratios in Baffin Bay and the Labrador Sea are higher than the ratios reported in the North Pacific (2.5-4.4 μmol mol^{-1}) and Southern Ocean (1.5-2.1 μmol mol^{-1}; Sunda, 1997). These differences could be attributed to the intra and inter-species variability of carbon:Fe quotas in diverse phytoplankton communities found in these disparate ocean environments.

In the deepest waters of Baffin Bay and the Labrador Sea, the DFe:AOU ratios deviate from the trends previously described (Fig. 10a). At BB2 station the concentrations suddenly decrease across BBDW (>1000 m) from 0.916±0.043 to 0.647±0.094 nmol kg^{-1} (Figs. 7 and 10a), and a large fraction of the remineralized DFe appears to be lost due to scavenging in this old and isolated water mass (Tang et al., 2004). In BBDW scavenging of DFe dominates over remineralization inputs, contrasting with nutrient distributions which increase steadily with depth reaching the highest concentrations measured in this study (Lehmann et al., 2019; Fig. 7). Both DFe and NO_3^- are released to the water column during the remineralization of organic particles, but only DFe undergoes scavenging; therefore, the DFe/NO_3^- ratio

provides information about scavenging regimens (lower value→stronger scavenging). DFe/NO_3^- ratios remained fairly constant (0.0495±0.0012) across the TrW and WGIW (remineralization > scavenging from 300-1000 m), decreasing notably with depth from the upper boundary of BBDW (0.0449) towards its base (0.0266; remineralization < scavenging). In the same way, DFe:AOU ratios in the Labrador Sea below ~2400 and ~2200 m at LS2 and K1, respectively, do not follow the trend described for LSW (Fig. 10a), and the concentrations decreased to 0.677±0.023 nmol kg^{-1} in bottom DSOW (Figs. 3a and 7). The DFe/NO_3^- ratios in the DSOW (> 2400 m) are lower (0.0447±0.0012) than in overlying waters (0.0507±0.0010), suggesting that scavenging of DFe is likely taking place, possibly as a consequence of the resuspension of sediments in this bottom water. The energetic flow of DSOW over bottom topography in the NASG is known to cause intense sediment resuspension, which results in elevated concentrations of dissolved Al in this water mass (Middag et al., 2015). Even though transmissivity data is not available for the deep casts (>1500 m) in the Labrador Sea, it is expected that the DSOW flow generates similar intense sediment resuspension events in this basin as suggested by the sharp decrease of particle reactive elements such as dissolved Pb and ^{230}Th at LS2 and K1 stations below 2500 m (Grenier et al., 2018; Colombo et al., 2019b). The comparably low DFe measured in bottom DSOW in the Irminger Basin and the NASG (0.630-0.740 and 0.500-0.590 nmol kg^{-1}, respectively; Rijkenberg et al., 2014; Schlitzer et al., 2018) associated with a thick nepheloid layer would reinforce the importance of enhanced bottom scavenging of DFe in DSOW due to sediment resuspension events. However, this behaviour contrasts with the sharp increase of DFe in near-bottom waters described in this study for the Canadian Arctic Archipelago and the Baffin Bay Slope, and with results from previous studies highlighting the importance sediment resuspension events as a source of DF in shelf environments (Lam and Bishop, 2008; Cullen et al., 2009; Klunder et al., 2012a; Hatta et al., 2015; Milne et al., 2017; Cheize et al., 2019; Vieira et al., 2019).

5.3.2 DMn distributions in deep ocean waters dominated by scavenging

In the Canada Basin below 300 m, DMn distribution are controlled primarily by the influence of the ACBC from 300 to 1000 m in the AL and scavenging removal in the CBDW. The concentrations measured in the AL (0.373±0.068 nmol kg^{-1}) in the Canada Basin are considerable higher than Atlantic-derived waters (0.120-0.240 nM) in the Eurasian Basin (Middag et al., 2011b) as result of the addition of Mn to the ACBC waters as they flow along the shallow shelves of the Siberian and Chukchi seas (Kondo et al., 2016). The FSB and BSB, the two main components of the AL, display a clear difference in their concentrations, with the warmer FSB (~500 m and σ_θ= 27.92) having lower values (0.327±0.012 nmol kg^{-1}) than the BSB (0.396±0.074 nmol kg^{-1}; ~600-1000 m and σ_θ= 28.00). This is similar to the difference previously described for DFe (section 5.3.1). Nevertheless, the noted difference in DFe distributions between stations CB2 and CB4 versus CB3 is not observed for DMn (Fig. 7), which shows similar distributions at the three sampled stations. This behaviour was also noted for in wBSW (section 5.2.1), where DMn concentrations do not change significantly across the basin.

In CBDW (>1200 m), DMn concentrations diminish with increasing depth, reaching uniformly low values 0.151±0.004 nmol kg^{-1} in bottom waters (>3000 m), the lowest concentrations measured in this study. The Canada Basin provides an excellent opportunity to study the scavenging dynamic of DMn, as well as DFe, especially within the CBDW. This old water is isolated from the ACBC by the Alpha-Mendeleev ridge complex, limiting advective trace metal inputs. In addition, the CBDW has not been recently ventilated, with an estimated water mass age of 500 years at ~4000 m (Macdonald et al., 1993; Timmermans et al., 2003; Tanhua et al., 2009; Fig. 10b). As the potential sources of trace metals to deep waters (advective sources, hydrothermal inputs and benthic fluxes) are non-existent or greatly reduced in CBDW, we can effectively isolate and estimate the effects of scavenging on trace metal distributions. We plot DMn concentrations (below 1200 m) against estimated water mass ages from Tanhua et al. (2009; Fig. 10b and c). A pseudo-first order scavenging model ($-dDMn/dt = kDMn$) is applied to fit our data: $DMn_t = DMn_0\, e^{-kt} + DM_{ss}$ (1), where DMn_t, DMn_0 *and* DM_{ss} are the

concentrations at time *t*, time *0* and steady-state, and *k* is the first-order scavenging constant (Yeats and Bewers, 1985; Statham et al., 1998; Richard et al., 2013). The calculated solutions of the scavenging model, using three different *k* values (0.015, 0.01, 0.008 $years^{-1}$; Weiss, 1977; Statham et al., 1998) and an assumed DMn "equilibrium" of 0.14 nmol kg^{-1}, show an excellent agreement with the observed data in CBDW (Fig. 10c). Various *k* values are chosen to fit the observed CBDW DMn data to account for different scavenging scenarios; high scavenging removal rates (e.g. 0.019 and 0.015 $years^{-1}$) were used by Weiss (1977) and Statham et al. (1998) to model DMn losses in the Galapagos Rift and in deep waters (~3000 m) from the Atlantic into the Indian and Pacific oceans, respectively. In these studies, most of the samples come from highly productive regions (e.g. Peruvian upwelling system, Greenland Sea, North Subarctic Atlantic) with high export production rates (Falkowski et al., 1998), rather than the extremely low productivity and export production rates typical of the Canada Basin (Hill et al., 2013; Varela et al., 2013; Brown et al., 2014; Crawford et al., 2015). Slightly lower scavenging removal rates (*k*= 0.010 and 0.008 $years^{-1}$) were also used in the equation (1) to fit our Canada Basin data (Fig. 10c). The best fit for the DMn data in CBDW is obtained with *k*= 0.010 $years^{-1}$, with a curvilinear relationship which describes the observed results with a standard error (measured vs. predicted concentrations) less than 3% and flattens out at about 400 years at CB3 and CB4 (0.147 and 0.150 nmol kg^{-1}; Fig. 10c). Scavenging dynamics of DMn in the CBDW are similar to those described by Statham et al. (1998; Fig. 10c); adding support to the hypothesis that DMn distributions in deep ocean waters approach a steady state concentration after approximately 400 years (if no external sources of Mn exist) reaching extremely low "background" concentrations (0.10-0.15 nM) in deep ocean waters (Statham et al., 1998; Middag et al., 2011b; Middag et al., 2011a; Hulten et al., 2017). Finally, the slightly lower scavenging rate constant used in this study (k= 0.010 $years^{-1}$), provides a better fit for Statham's model for the stations located in the Sargasso Sea and Southern Ocean (low productivity and export production regions) which were overestimated using a higher k value (0.015 $years^{-1}$; Fig. 10c).

Dissolved Mn concentrations below 300 m in Baffin Bay and the Labrador Sea, in contrast to DFe, do not show a significant correlation with AOU. This could be explained by the greater elemental stoichiometry of Fe relative to Mn in marine phytoplankton (2:1) and diminished Fe scavenging owing to complexation by organic ligands (Ho et al., 2003; Gerringa et al., 2015). In the highly productive Baffin Bay waters, Mn is indeed released to the dissolved phase during the remineralization of sinking particles, but rapid scavenging of DMn potentially obscures any correlation with AOU in WGIW (~300-1000 m and σ_θ= 27.35-27.63). The only station where DMn concentrations show a significant positive relationship with AOU is BB1 (*DMn= [(0.0024 AOU) / µmol L^{-1} + 0.368] nmol kg^{-1};* R^2= 0.81 and *p-value*< 0.05). Interestingly, the Mn:C ratio of sinking organic matter at BB1 (3.8 µmol mol^{-1}) derived from the DMn:AOU relationship and the AOU:C ratio agrees with the Mn:C ratio (4.1 µmol mol^{-1}) estimated using the Fe:C in Baffin Bay (8.3 µmol mol^{-1}) and the 2:1 Fe/Mn stoichiometry. The nearly uniform distributions of DMn in WGIW (Fig. 7) are associated with a dynamic equilibrium between remineralization inputs and scavenging removal. The lower concentrations measured at BB2 station (0.416±0.005 nmol kg^{-1}) relative to the stations BB1 and BB3 (0.600±0.036 and 0.521±0.011nmol kg^{-1}) are related with the greater proportion of old Baffin Bay water in the former station, as described in the section 5.3.1. The sudden increase of DMn at near-bottom waters at stations BB1 and BB2 (0.768±0.057 and 0.736±0.048 nmol kg^{-1}) and the extremely high concentration measured at BB3 (4.20±0.008 nmol kg^{-1}) is also accompanied by the spike of particulate Fe and Mn concentrations and a decrease of the particle reactive radionuclide ^{230}Th (Li, 2017; Grenier et al., 2018), which strongly suggest that particle resuspension at the sediment-water boundary is driving the DMn increase.

The DMn concentrations in BBDW (~700-2300 m and σ_θ >27.63) are low and steadily decrease with increasing depth from 700 to 1900 m (0.314±0.103 to 0.244±0.032 nmol kg^{-1}), distinguishing them from overlying WGIW concentrations (0.416±0.005 nmol kg^{-1}; Fig. 7). Like DFe (section 5.3.1), the decrease of DMn in BBDW is attributed to scavenging removal in these old and isolated bottom waters. The origin of BBDW has been under discussion for many decades, and the ventilation age of these deep waters

(77-1450 years) is still uncertain (Tang et al., 2004; Lehmann et al., 2019). Insights from the scavenging dynamic of DMn in the Canada Basin could help to better constrain the large uncertainties in the BBDW age. Dissolved Mn in deep waters reaches a background concentration of 0.10 to 0.15 nmol kg^{-1} after approximately 400 years, provided no external sources are present (Fig. 10c). In Baffin Bay, external sources of Mn to BBDW are assumed to be negligible since this bay is isolated from Arctic and Atlantic outflows by shallow (< 150 m) and narrow passages in the Canadian Arctic Archipelago and by the Davis Strait (< 650 m), and the benthic fluxes of DMn are restricted to near-bottom waters (Fig. 7). Additionally, the entrainment of high DMn from shallower waters is also unlikely considering that convective mixing is restricted to the upper 400 m (Colombo et al., 2019b), and below this depth the WGIW and BBDW temperature profiles can be clearly distinguished from each other (Fig. 7). The lowest concentrations measured in BBDW (0.244±0.032 nmol kg^{-1}) are far from the background level of Mn, which indicate that these waters have not reached the equilibrium concentration, and therefore they are younger than ~400 years. Considering that the measured concentrations in the upper boundary of BBDW (0.314±0.103 nmol kg^{-1}) are comparable to those of CBDW (0.269-0.336 nmol kg^{-1}), we can roughly estimate the age which will reproduce the DMn measured in BBDW using the equation (1). Based on the scavenging model previously described, using k values from 0.008 to 0.015 $years^{-1}$ and assuming that external sources of Mn are negligible, an estimate of age 120-190 years would reproduce the 0.244 nmol kg^{-1} measured in BBDW at ~1900 m. These estimates are approximately one order of magnitude lower than the upper limit range of estimated residence time (1450 years), and comparable to the lower range (77-455 years) estimated using a time dependent ^{3}He/ Tritium two-box model (Top et al., 1980).

Finally, the distributions of DMn in Labrador Sea deep waters (> 300m), are characterized by a steady decrease in concentration with increasing depth across multiple water masses (LSW-2015, ISW, LSW-87/94 and NEADW) until about 2500 m (σ_θ= 27.86) where the lowest concentrations were measured (0.306-0.330 nmol kg^{-1}; Fig. 7). Differences in DMn concentrations across LSW-2015 waters

(~400-1000 m and σ_θ= 27.71-27.74) are noticed between LS2 and K1 stations. In these stations DMn mirrors the temperature and oxygen profiles (Fig. 7), with higher DMn concentrations measured in the cooler, fresher and more oxygenated LSW-2015 waters at K1 than at LS2. Below the ISW, DMn distributions at stations LS2 and K1 follow similar trends across LSW-87/94, NEADW and DSOW waters, and their concentrations are a result of the combined effects of scavenging removal and the initial concentrations of these water masses at the time they were last ventilated. The old LSW-87/94 waters have slightly higher concentrations (0.367±0.023 nmol kg^{-1}) than the NEADW (0.338±0.014 nmol kg^{-1}), despite the fact that the LSW-87/94 was ventilated approximately 30 years ago (Azetsu-Scott et al., 2005; Yashayaev and Clarke, 2008) compared to the more recently ventilated NEADW (~11-13 years; Azetsu-Scott et al., 2005). This apparent inconsistency is related to differences in surface DMn concentration where these water masses were ventilated, with relatively higher concentration in the Labrador Sea (0.450-0.850 nmol kg^{-1}) compared to the Irminger and Iceland basins (~0.20-0.50 nM; Achterberg et al., 2018). The modest increase of DMn (0.372±0.013 nmol kg^{-1}) in bottom DSOW waters (>2500 m and σ_θ >27.86) at stations LS2 and K1 is potentially linked to sediment resuspension events generated by the energetic flow of DSOW over bottom topography. It is important to highlight that DFe concentrations were uniformly low in this water mass (section 5.3.1); this difference between DMn and DFe in the DSOW has been previously observed in the Irminger Basin and the NASG (Rijkenberg et al., 2014; Hulten et al., 2017), reporting similar values of DMn (~0.35-0.40 nM) to those measured in this study. Over much of the sampled area in the Canadian Arctic Ocean, the noticeable rise of DFe concentrations in near-bottom waters are associated with intense sediment resuspension events (e.g. the Canadian Arctic Archipelago, the Baffin Bay slope region) and are accompanied by an increase of DMn. However, the contrasting behavior described for the DSOW, where the bottom waters were enriched in DMn, but not in DFe, is also found in BBDW at the deep BB2 station. Consequently, further research, including iron isotopic measurements and size partitioning analysis (soluble, colloidal and dissolved fractions), is required to unravel the processes that result in the apparent decoupling of DMn and DFe in the deepest waters sampled in Baffin Bay and the Labrador Sea.

5.4 Conclusions

We present distributions of dissolved Fe and Mn in the Canadian Arctic Ocean from the Canada Basin to the Labrador Sea. High resolution profiles were sampled during the Canadian GEOTRACES Arctic cruise in 2015. Fresh water sources, mostly riverine inputs, control the surface distributions of these metals in the Canadian Arctic Ocean; especially high concentrations were found in the Canadian Arctic Archipelago (CAA), a coastal region receiving a large flux of freshwater from numerous river systems. Surface waters in the Labrador Sea stand out with their extremely low DFe and DMn concentrations (0.106-0.362 and 0.450-1.09 nmol kg^{-1}), that likely result from reduced freshwater inputs and increased phytoplankton uptake in the region (Fig. 11). Relatively high DFe and DMn are present in subsurface waters (~100-300 m) across the Canada Basin, the CAA and Baffin Bay; these distinctive signatures are advected from the Chukchi Sea and the CAA, where increased concentrations reflect benthic fluxes and continental shelf-seawater interactions in these shallow environments (Fig. 11). The distributions of DFe and DMn in deep waters are regulated by complex interactions between removal processes (e.g. scavenging, oxidative precipitation) and inputs of these trace metals (e.g. remineralization, advection, adsorption/desorption equilibrium dynamics between particulate and dissolved phase). As a general trend, DFe distributions in Baffin Bay and the Labrador Sea below 300 m are regulated by an interplay between remineralization inputs and scavenging removal in the deepest waters, while in the Canada Basin, an extremely low productivity region, the remineralization of sinking organic particles does not appear to be a significant source of trace metals to deep waters (Fig. 11). The distributions of DFe and DMn in the deep Canada Basin waters are greatly influenced by the advection of these metals in the Arctic Circumpolar Boundary Current, and the subsequent scavenging in deeper waters. The vertical distribution of DMn in the deep basins is predominantly controlled by scavenging removal, and a pseudo-first order scavenging model best explains the uniformly low concentrations (0.151±0.004 nmol kg^{-1}) measured in the deep and old (>3000 m and ~400 years) Canada Basin Deep Waters. The consistent

965 scavenging behavior of DMn observed in deep world oceans and in the Canada Basin allows to better
966 constrain the ages of Baffin Bay Deep Waters, which have been under debate since 1980's.

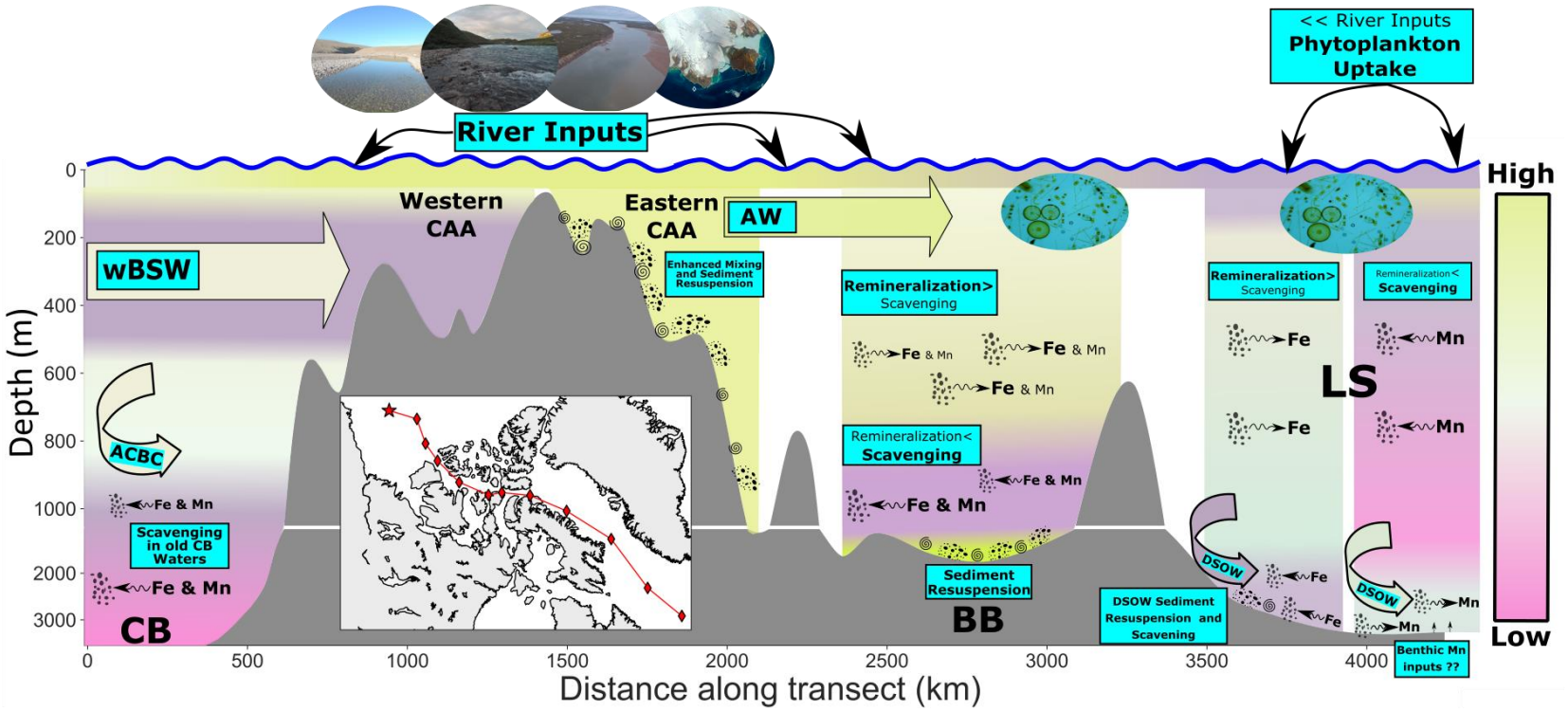

Fig. 11. Conceptual scheme displaying the concentrations and key processes controlling the distributions of dissolved Fe and Mn in the Canadian Arctic Ocean. CB: Canada Basin, CAA: Canadian Artic Archipelago, BB: Baffin Bay, LS: Labrador Sea, wBSW: winter Bering Sea Water, ACBC: Arctic Circumpolar Boundary Current, AW: Arctic Water, DSOW: Denmark Strait Overflow Water.

ACKNOWLEDGMENTS

This work was supported by the Natural Sciences and Engineering Research Council of Canada (Grant NSERC-CCAR) and the Northern Scientific Training Program. We thank the captain and crew of the *CCGS Amundsen* as well as Chief Scientist Roger Francois and the trace metal rosette group (Priyanka Chandan, Kang Wang, Kathleen Munson, Jingxuan Li, David Semeniuk, Dave Janssen, Rowan Fox and Kathryn Purdon) for their assistance in sample collection. We also thank ArcticNet; Jean-Eric Tremblay's group for providing the nutrient data for the Canadian GEOTRACES 2015 cruise. The Pacific Centre for Isotopic and Geochemical Research and its staff are thanked for assistance with sample analyses. We thank three anonymous reviewers for their thoughtful comments, which helped to improve this manuscript.

Research Data

The full data set of iron and manganese concentrations collected and discussed in this study are provided in the Electronic Annex, Tables EA2 and EA3.

Electronic Annex. Supplementary Material

Figs. EA1-EA6 and Tables EA1-EA3 are available for this manuscript in the supplementary material.

References

Achterberg E. P., Steigenberger S., Marsay C. M., LeMoigne F. A. C., Painter S. C., Baker A. R., Connelly D. P., Moore C. M., Tagliabue A. and Tanhua T. (2018) Iron Biogeochemistry in the High Latitude North Atlantic Ocean. *Sci. Rep.* **8**, 1283. Available at: http://www.nature.com/articles/s41598-018-19472-1.

Aguilar-Islas A. M., Rember R., Nishino S., Kikuchi T. and Itoh M. (2013) Partitioning and lateral transport of iron to the Canada Basin. *Polar Sci.* **7**, 82–99. Available at: http://dx.doi.org/10.1016/j.polar.2012.11.001.

Aksenov Y., Ivanov V. V., Nurser A. J. G., Bacon S., Polyakov I. V., Coward A. C., Naveira-Garabato A. C. and Beszczynska-Moeller A. (2011) The arctic circumpolar boundary current. *J. Geophys. Res. Ocean.* **116**, 1–28.

Alkire M. B., Jacobson A. D., Lehn G. O., Macdonald R. W. and Rossi M. W. (2017) On the geochemical heterogeneity of rivers draining into the straits and channels of the Canadian Arctic Archipelago. *J. Geophys. Res. Biogeosciences* **122**, 2527–2547.

Azetsu-Scott K., Jones E. P. and Gershey R. M. (2005) Distribution and ventilation of water masses in the Labrador Sea inferred from CFCs and carbon tetrachloride. *Mar. Chem.* **94**, 55–66.

Bergquist B. A. and Boyle E. A. (2006) Dissolved iron in the tropical and subtropical Atlantic Ocean. *Global Biogeochem. Cycles* **20**, 1–14.

Beszczynska-Möller A., Woodgate R., Lee C., Melling H. and Karcher M. (2011) A Synthesis of Exchanges Through the Main Oceanic Gateways to the Arctic Ocean. *Oceanography* **24**, 82–99. Available at: http://dx.doi.org/10.5670/oceanog.2011.80.

Bown J., van Haren H., Meredith M. P., Venables H. J., Laan P., Brearley J. A. and de Baar H. J. W. (2018) Evidences of strong sources of DFe and DMn in Ryder Bay, Western Antarctic Peninsula. *Philos. Trans. R. Soc. A Math. Phys. Eng. Sci.* **376**, 1–18.

Boyd P. W. and Ellwood M. J. (2010) The biogeochemical cycle of iron in the ocean. *Nat. Geosci.* **3**, 675–682. Available at: http://dx.doi.org/10.1038/ngeo964.

Boyle E. A., Bergquist B. A., Kayser R. A. and Mahowald N. (2005) Iron, manganese, and lead at Hawaii Ocean Time-series station ALOHA: Temporal variability and an intermediate water hydrothermal plume. *Geochim. Cosmochim. Acta* **69**, 933–952.

Bring A., Fedorova I., Dibike Y., Hinzman L., Mård J., Mernild S. H., Prowse T., Semenova O., Stuefer S. L. and Woo M. K. (2016) Arctic terrestrial hydrology: A synthesis of processes, regional effects, and research challenges. *J. Geophys. Res. Biogeosciences* **121**, 621–649.

Brown K. A., McLaughlin F., Tortell P. D., Varela D. E., Yamamoto-Kawai M., Hunt B. and Francois R. (2014) Determination of particulate organic carbon sources to the surface mixed layer of the Canada Basin, Arctic Ocean. *J. Geophys. Res. Ocean.* **119**, 1084–1102.

Bruland K. W. K., Donat J. R. J. and Hutchins D. A. (1991) Interactive Influences of Bioactive Trace-Metals on Biological Production in Oceanic Waters. *Limnol. Oceanogr.* **36**, 1555–1577.

Buck K. N., Sedwick P. N., Sohst B. and Carlson C. A. (2018) Organic complexation of iron in the eastern tropical South Pacific: Results from US GEOTRACES Eastern Pacific Zonal Transect (GEOTRACES cruise GP16). *Mar. Chem.* **201**, 229–241. Available at:

https://doi.org/10.1016/j.marchem.2017.11.007.

Campbell J. A. and Yeats P. A. (1982) The distribution of manganese , iron , nickel , copper and cadmium in the waters of Baffin Bay and the Canadian Arctic Archipelago. *Oceanol. Acta* **5**, 161–168.

Chang B. X. and Devol A. H. (2009) Seasonal and spatial patterns of sedimentary denitrification rates in the Chukchi sea. *Deep. Res. Part II Top. Stud. Oceanogr.* **56**, 1339–1350.

Cheize M., Planquette H. F., Fitzsimmons J. N., Pelleter E., Sherrell R. M., Lambert C., Bucciarelli E., Sarthou G., Le Goff M., Liorzou C., Chéron S., Viollier E. and Gayet N. (2019) Contribution of resuspended sedimentary particles to dissolved iron and manganese in the ocean: An experimental study. *Chem. Geol.* **511**, 389–415. Available at: https://doi.org/10.1016/j.chemgeo.2018.10.003.

Cid A. P., Nakatsuka S. and Sohrin Y. (2012) Stoichiometry among bioactive trace metals in the Chukchi and Beaufort Seas. *J. Oceanogr.* **68**, 985–1001.

Colombo M., Brown K. A., De Vera J., Bergquist B. A. and Orians K. J. (2019a) Trace metal geochemistry of remote rivers in the Canadian Arctic Archipelago. *Chem. Geol.* **525**, 479–491. Available at: https://linkinghub.elsevier.com/retrieve/pii/S0009254119303742.

Colombo M., Rogalla B., Myers P. G., Allen S. E. and Orians K. J. (2019b) Tracing Dissolved Lead Sources in the Canadian Arctic: Insights from the Canadian GEOTRACES Program. *ACS Earth Sp. Chem.* **3**, 1302–1314.

Crawford D. W., Wyatt S. N., Wrohan I. A., Cefarelli A. O., Giesbrecht K. E., Kelly B. and Varela D. E. (2015) Low particulate carbon to nitrogen ratios in marine surface waters of the Arctic. *Global Biogeochem. Cycles* **29**, 2021–2033.

Cullen J. T., Chong M. and Ianson D. (2009) British columbian continental shelf as a source of dissolved iron to the subarctic northeast Pacific Ocean. *Global Biogeochem. Cycles* **23**, 1–12.

Cuny J., Rhines P. B. and Kwok R. (2005) Davis Strait volume, freshwater and heat fluxes. *Deep. Res. Part I Oceanogr. Res. Pap.* **52**, 519–542.

Cuny J., Rhines P. B., Niiler P. P. and Bacon S. (2002) Labrador Sea Boundary Currents and the Fate of the Irminger Sea Water. *J. Phys. Oceanogr.* **32**, 627–647. Available at: http://dx.doi.org/10.1175/1520-0485(2002)032%3C0627:lsbcat%3E2.0.co;2.

Curry B., Lee C. M. and Petrie B. (2011) Volume, Freshwater, and Heat Fluxes through Davis Strait, 2004–05*. *J. Phys. Oceanogr.* **41**, 429–436.

Cutter G. R., Andersson P., Codispoti L., Croot P., Francois R., Lohan M. C., Obata H., van der Loeff M., François R., Lohan M. C., Obata H., Rutgers v. d. Loeff M., Francois R., Lohan M. C., Obata H. and van der Loeff M. (2010) *Sampling and Sample-handling Protocols for GEOTRACES Cruises*., Available at: http://www.geotraces.org/library/geotraces-policies/170-sampling-and-sample-handling-protocols-for-geotraces-cruises.

Duce R. A., Liss P. S., Merrill J. T., Atlas E. L., Buat-Menard P., Hicks B. B., Miller J. M., Prospero J. M., Arimoto R., Church T. M., Ellis W., Galloway J. N., Hansen L., Jickells T. D., Knap A. H., Reinhardt K. H., Schneider B., Soudine A., Tokos J. J., Tsunogai S., Wollast R. and Zhou M. (1991) The atmospheric input of trace species to the world ocean. *Global Biogeochem. Cycles* **5**, 193–259.

Falkowski P. G., Barber R. T. and Smetacek V. (1998) Biogeochemical Controls and Feedbacks on

Ocean Primary Production. *Science (80-.).* **281**, 200–206.

Field M. P. and Sherrell R. M. (2000) Dissolved and particulate Fe in a hydrothermal plume at 9°45′N, East Pacific Rise: *Geochim. Cosmochim. Acta* **64**, 619–628.

Fischer J., Schott F. A. and Dengler M. (2004) Boundary Circulation at the Exit of the Labrador Sea. *J. Phys. Oceanogr.* **34**, 1548–1570.

Fitzsimmons J. N., Carrasco G. G., Wu J., Roshan S., Hatta M., Measures C. I., Conway T. M., John S. G. and Boyle E. A. (2015) Partitioning of dissolved iron and iron isotopes into soluble and colloidal phases along the GA03 GEOTRACES North Atlantic Transect. *Deep. Res. Part II Top. Stud. Oceanogr.* **116**, 130–151. Available at: http://dx.doi.org/10.1016/j.dsr2.2014.11.014.

Fitzsimmons J. N., John S. G., Marsay C. M., Hoffman C. L., Nicholas S. L., Toner B. M., German C. R. and Sherrell R. M. (2017) Iron persistence in a distal hydrothermal plume supported by dissolved-particulate exchange. *Nat. Geosci.* **10**, 195–201.

Fitzsimmons J. N., Zhang R. and Boyle E. A. (2013) Dissolved iron in the tropical North Atlantic Ocean. *Mar. Chem.* **154**, 87–99. Available at: http://dx.doi.org/10.1016/j.marchem.2013.05.009.

Frajka-Williams E., Rhines P. B., Ã E. F., Rhines P. B. and Strait D. (2010) Physical controls and interannual variability of the Labrador Sea spring phytoplankton bloom in distinct regions. *Deep. Res. Part I Oceanogr. Res. Pap.* **57**, 541–552.

Fung I. Y., Meyn S. K., Tegen I., Doney S. C., John J. G. and Bishop J. K. B. (2000) Iron supply and demand in the upper ocean. *Global Biogeochem. Cycles* **14**, 281–295.

Gerringa L. J. A., Rijkenberg M. J. A., Schoemann V., Laan P. and de Baar H. J. W. (2015) Organic complexation of iron in the West Atlantic Ocean. *Mar. Chem.* **177**, 434–446. Available at: http://dx.doi.org/10.1016/j.marchem.2015.04.007.

Granger J., Sigman D. M., Gagnon J., Tremblay J.-E. and Mucci A. (2018) On the properties of the Arctic Halocline and deep water masses of the Canada Basin from nitrate isotope ratios. *J. Geophys. Res. Ocean.* **123**, 1–16. Available at: http://doi.wiley.com/10.1029/2018JC014110.

Grenier M., Francois R., Soon M., Baconnais I., Pham V. and Jeandel C. (2018) Ocean circulation and land-ocean exchanges off the north eastern Canadian coasts as told by dissolved geochemical tracers. In *Goldschmidt Abstracts* p. 2018 880.

Grenier M., François R., Soon M., Rutgers van der Loeff M., Yu X., Valk O., Not C., Moran S. B., Edwards R. L., Lu Y., Lepore K. and Allen S. E. (2019) Changes in Circulation and Particle Scavenging in the Amerasian Basin of the Arctic Ocean over the Last Three Decades Inferred from the Water Column Distribution of Geochemical Tracers. *J. Geophys. Res. Ocean.* **124**, 9338–9363.

Gruber N. and Sarmiento J. L. (1997) Global patterns of marine nitrogen fixation and denitrification. *Global Biogeochem. Cycles* **11**, 235–266.

Guay C. K. H., McLaughlin F. A. and Yamamoto-Kawai M. (2009) Differentiating fluvial components of upper Canada Basin waters on the basis of measurements of dissolved barium combined with other physical and chemical tracers. *J. Geophys. Res.* **114**, 1–17. Available at: http://doi.wiley.com/10.1029/2008JC005099.

Guieu C., Duce R. and Arimoto R. (1994) Dissolved input of manganese to the ocean: Aerosol source. *J. Geophys. Res. Atmos.* **99**, 18789–18800. Available at: http://dx.doi.org/10.1029/94JD01120.

Hannah C. G., Dupont F. and Dunphy M. (2009) Polynyas and Tidal Currents in the Canadian Arctic Archipelago. *Arctic* **62**, 83–95.

Hansard S. P., Landing W. M., Measures C. I. and Voelker B. M. (2009) Dissolved iron(II) in the Pacific Ocean: Measurements from the PO2 and P16N CLIVAR/CO2repeat hydrography expeditions. *Deep. Res. Part I Oceanogr. Res. Pap.* **56**, 1117–1129. Available at: http://dx.doi.org/10.1016/j.dsr.2009.03.006.

Hatta M., Measures C. I., Wu J., Roshan S., Fitzsimmons J. N., Sedwick P. and Morton P. (2015) An overview of dissolved Fe and Mn distributions during the 2010-2011 U.S. GEOTRACES north Atlantic cruises: GEOTRACES GA03. *Deep. Res. Part II Top. Stud. Oceanogr.* **116**, 117–129.

Henkel S., Kasten S., Hartmann J. F., Silva-Busso A. A. and Staubwasser M. (2018) Iron cycling and stable Fe isotope fractionation in Antarctic shelf sediments, King George Island. *Geochim. Cosmochim. Acta* **237**, 320–338.

Hill V. J., Matrai P. A., Olson E., Suttles S., Steele M., Codispoti L. A. and Zimmerman R. C. (2013) Synthesis of integrated primary production in the Arctic Ocean: II. In situ and remotely sensed estimates. *Prog. Oceanogr.* **110**, 107–125. Available at: http://dx.doi.org/10.1016/j.pocean.2012.11.005.

Hioki N., Kuma K., Morita Y., Sasayama R., Ooki A., Kondo Y., Obata H., Nishioka J., Yamashita Y., Nishino S., Kikuchi T. and Aoyama M. (2014) Laterally spreading iron, humic-like dissolved organic matter and nutrients in cold, dense subsurface water of the Arctic Ocean. *Sci. Rep.* **4**, 1–9.

Ho T. Y., Finkel Z. V, Milligan A. J., Wyman K., Falkowski P. G. and Morel F. M. M. (2003) The elemental composition of some marine phytoplankton. *J. Phycol.* **39**, 1145–1159.

Hölemann J. A., Schirmacher M. and Prange A. (2005) Seasonal variability of trace metals in the Lena River and the southeastern Laptev Sea: Impact of the spring freshet. *Glob. Planet. Change* **48**, 112–125.

Hughes K. G., Klymak J. M., Hu X. and Myers P. G. (2017) Water mass modification and mixing rates in a 1/12° simulation of the Canadian Arctic Archipelago. *J. Geophys. Res. Ocean.* **122**, 803–820.

Hughes K. G., Klymak J. M., Williams W. J. and Melling H. (2018) Tidally Modulated Internal Hydraulic Flow and Energetics in the Central Canadian Arctic Archipelago. *J. Geophys. Res. Ocean.* **123**, 5210–5229.

Hulten M. Van, Middag R., Dutay J. C., Baar H. De, Roy-Barman M., Gehlen M., Tagliabue A., Sterl A., Lsce E., Orme C. E. A., Van Hulten M., Middag R., Dutay J. C., De Baar H., Roy-Barman M., Gehlen M., Tagliabue A. and Sterl A. (2017) Manganese in the west Atlantic Ocean in the context of the first global ocean circulation model of manganese. *Biogeosciences* **14**, 1123–1152.

Jackson S. L., Spence J., Janssen D. J., Ross A. R. S. and Cullen J. T. (2018) Determination of Mn, Fe, Ni, Cu, Zn, Cd and Pb in seawater using offline extraction and triple quadrupole ICP-MS/MS. *J. Anal. At. Spectrom.* **33**, 304–313. Available at: http://dx.doi.org/10.1039/C7JA00237H.

Jeandel C. (2016) Overview of the mechanisms that could explain the "Boundary Exchange" at the land-ocean contact. *Philos. Trans. R. Soc. A Math. Phys. Eng. Sci.* **374**.

Jeandel C. and Oelkers E. H. (2015) The influence of terrigenous particulate material dissolution on ocean chemistry and global element cycles. *Chem. Geol.* **395**, 50–66. Available at:

http://dx.doi.org/10.1016/j.chemgeo.2014.12.001.

Jickells T. D., An Z. S., Andersen K. K., Baker A. R., Bergametti C., Brooks N., Cao J. J., Boyd P. W., Duce R. A., Hunter K. A., Kawahata H., Kubilay N., LaRoche J., Liss P. S., Mahowald N., Prospero J. M., Ridgwell A. J., Tegen I. and Torres R. (2005) Global iron connections between desert dust, ocean biogeochemistry, and climate. *Science (80-.).* **308**, 67–71.

John S. G., Helgoe J., Townsend E., Weber T., DeVries T., Tagliabue A., Moore K., Lam P., Marsay C. M. and Till C. (2018) Biogeochemical cycling of Fe and Fe stable isotopes in the Eastern Tropical South Pacific. *Mar. Chem.* **201**, 66–76. Available at: https://doi.org/10.1016/j.marchem.2017.06.003.

Johnson K. S., Chavez F. P. and Friederich G. E. (1999) Continental-shelf sediment as a primary source of iron for coastal phytoplankton. *Nature* **398**, 697–700.

Johnson K. S., Michael Gordon R. and Coale K. H. (1997) What controls dissolved iron concentrations in the world ocean? *Mar. Chem.* **57**, 137–161.

Jones E. P. (2003) Tracing Pacific water in the North Atlantic Ocean. *J. Geophys. Res.* **108**, 3116. Available at: http://doi.wiley.com/10.1029/2001JC001141.

Kadko D., Aguilar-Islas A., Bolt C., Buck C. S., Fitzsimmons J. N., Jensen L. T., Landing W. M., Marsay C. M., Rember R., Shiller A. M., Whitmore L. M. and Anderson R. F. (2018) The residence times of trace elements determined in the surface Arctic Ocean during the 2015 US Arctic GEOTRACES expedition. *Mar. Chem.*, 1–14. Available at: https://linkinghub.elsevier.com/retrieve/pii/S0304420318301993.

Kaupp L. J., Measures C. I., Selph K. E., Mackenzie F. T., Johanna L., Measures C. I., Selph K. E. and Mackenzie F. T. (2011) The distribution of dissolved Fe and Al in the upper waters of the Eastern Equatorial Pacific. *Deep. Res. Part II Top. Stud. Oceanogr.* **58**, 296–310. Available at: http://dx.doi.org/10.1016/j.dsr2.2010.08.009.

Klar J. K., Statham P. J., Woodward E. M. S., Silburn B., Connelly D. P., Homoky W. B., Cooper M. J., Harris E. L., Lichtschlag A., James R. H., Graves C., Birchill A. J. and Chever F. (2017) Stability of dissolved and soluble Fe(II) in shelf sediment pore waters and release to an oxic water column. *Biogeochemistry* **135**, 49–67.

Klunder M. B., Bauch D., Laan P., De Baar H. J. W., Van Heuven S. and Ober S. (2012a) Dissolved iron in the Arctic shelf seas and surface waters of the central Arctic Ocean: Impact of Arctic river water and ice-melt. *J. Geophys. Res. Ocean.* **117**, 1–18.

Klunder M. B., Laan P., Middag R., De Baar H. J. W. and Bakker K. (2012b) Dissolved iron in the Arctic Ocean: Important role of hydrothermal sources, shelf input and scavenging removal. *J. Geophys. Res. Ocean.* **117**, 1–17.

Klunder M. B., Laan P., Middag R., De Baar H. J. W. and van Ooijen J. C. (2011) Dissolved iron in the Southern Ocean (Atlantic sector). *Deep. Res. Part II Top. Stud. Oceanogr.* **58**, 2678–2694. Available at: http://dx.doi.org/10.1016/j.dsr2.2010.10.042.

Kondo Y., Obata H., Hioki N., Ooki A., Nishino S., Kikuchi T. and Kuma K. (2016) Transport of trace metals (Mn, Fe, Ni, Zn and Cd) in the western Arctic Ocean (Chukchi Sea and Canada Basin) in late summer 2012. *Deep Sea Res. Part I Oceanogr. Res. Pap.* **116**, 236–252. Available at: http://dx.doi.org/10.1016/j.dsr.2016.08.010.

Lam P. J. and Bishop J. K. B. (2008) The continental margin is a key source of iron to the HNLC North Pacific Ocean. *Geophys. Res. Lett.* **35**, 1–5.

Lammers R. B., Shiklomanov A. I., Vörösmarty C. J., Fekete B. M. and Peterson B. J. (2001) Assessment of contemporary Arctic river runoff based on observational discharge records. *J. Geophys. Res.* **106**, 3321.

Landing W. M. and Bruland K. W. (1980) Manganese in the North Pacific. *Earth Planet. Sci. Lett.* **49**, 45–56.

Landing W. M. and Bruland K. W. (1987) The contrasting biogeochemistry of iron and manganese in the Pacific Ocean. *Geochim. Cosmochim. Acta* **51**, 29–43.

Lansard B., Mucci A., Miller L. A., MacDonald R. W. and Gratton Y. (2012) Seasonal variability of water mass distribution in the southeastern Beaufort Sea determined by total alkalinity and δ18O. *J. Geophys. Res. Ocean.* **117**, 1–19.

Lehmann N., Kienast M., Granger J., Bourbonnais A., Altabet M. A. and Tremblay J. -É. (2019) Remote Western Arctic Nutrients Fuel Remineralization in Deep Baffin Bay. *Global Biogeochem. Cycles*, 2018GB006134. Available at: https://onlinelibrary.wiley.com/doi/abs/10.1029/2018GB006134.

Lenaerts J. T. M., Van Angelen J. H., Van Den Broeke M. R., Gardner A. S., Wouters B. and Van Meijgaard E. (2013) Irreversible mass loss of Canadian Arctic Archipelago glaciers. *Geophys. Res. Lett.* **40**, 870–874.

Li J. (2017) Particulate trace metals & iron availability to phytoplankton in a changing Arctic Ocean. University of British Columbia. Available at: //open.library.ubc.ca/collections/ubctheses/24/items/1.0348666.

Lozier M. S., Bacon S., Bower A. S., Cunningham S. A., De Jong M. F., De Steur L., De Young B., Fischer J., Gary S. F., Greenan B. J. W., Heimbmbach P., Holliday N. P., Houpert L., Inall M. E., Johns W. E., Johnson H. L., Karstensen J., Li F., Lin X., Mackay N., Marshall D. P., Mercier H., Myers P. G., Pickart R. S., Pillar H. R., Straneo F., Thierry V., Weller R. A., Williams R. G., Wilson C., Yang J., Zhao J. and Zika J. D. (2017) Overturning in the Subpolar north Atlantic program: A new international ocean observing system. *Bull. Am. Meteorol. Soc.* **98**, 737–752.

Macdonald R. W., Carmack E. C. and Wallace D. W. R. (1993) Tritium and Radiocarbon Dating of Canada Basin Deep Waters. *Science (80-.).* **259**, 103–104.

Maldonado M. T. and Price N. M. (1996) Influence of N substrate on Fe requirements of marine centric diatoms. *Mar. Ecol. Prog. Ser.* **141**, 161–172.

Marsay C. M., Aguilar-Islas A., Fitzsimmons J. N., Hatta M., Jensen L. T., John S. G., Kadko D., Landing W. M., Lanning N. T., Morton P. L., Pasqualini A., Rauschenberg S., Sherrell R. M., Shiller A. M., Twining B. S., Whitmore L. M., Zhang R. and Buck C. S. (2018a) Dissolved and particulate trace elements in late summer Arctic melt ponds. *Mar. Chem.* **204**, 70–85. Available at: https://doi.org/10.1016/j.marchem.2018.06.002.

Marsay C. M., Kadko D., Landing W. M., Morton P. L., Summers B. A. and Buck C. S. (2018b) Concentrations, provenance and flux of aerosol trace elements during US GEOTRACES Western Arctic cruise GN01. *Chem. Geol.* **502**, 1–14. Available at: https://doi.org/10.1016/j.chemgeo.2018.06.007.

Martin J. H. and Fitzwater S. E. (1988) Iron-deficiency limits phytoplankton growth in the northeast Pacific subarctic. *Nature* **331**, 341–343. Available at: http://www.nature.com/doifinder/10.1038/331341a0.

Martin J. H., Knauer G. A., Karl D. M. and Broenkow W. W. (1987) VERTEX: carbon cycling in the northeast Pacific. *Deep Sea Res.* **34**, 267–285.

Martin J.H., Gordon M.R. F. E. S. (1991) Iron Limitation? *Limnol. Oceanogr.* **36**, 1793–1802. Available at: http://doi.wiley.com/10.4319/lo.1991.36.8.1793%0Ahttp://onlinelibrary.wiley.com/store/10.4319/lo.1991.36.8.1793/asset/lno19913681793.pdf?v=1&t=j6qdk51h&s=456915f948d9c4ef90e914c1583d2396c4bfe2b6.

McLaughlin F. A., Carmack E. C., Macdonald R. W., Melling H., Swift J. H., Wheeler P. A., Sherr B. F. and Sherr E. B. (2004) The joint roles of Pacific and Atlantic-origin waters in the Canada Basin, 1997-1998. *Deep. Res. Part I Oceanogr. Res. Pap.* **51**, 107–128.

McLaughlin F., Shimada K., Carmack E., Itoh M. and Nishino S. (2005) The hydrography of the southern Canada Basin, 2002. *Polar Biol.* **28**, 182–189.

Measures C. I., Landing W. M., Brown M. T. and Buck C. S. (2008) High-resolution Al and Fe data from the Atlantic Ocean CLIVAR-CO2 Repeat Hydrography A16N transect: Extensive linkages between atmospheric dust and upper ocean geochemistry. *Global Biogeochem. Cycles* **22**, 1–10.

Mendez J., Guieu C. and Adkins J. (2010) Atmospheric input of manganese and iron to the ocean: Seawater dissolution experiments with Saharan and North American dusts. *Mar. Chem.* **120**, 34–43.

Michel C., Hamilton J., Hansen E., Barber D., Reigstad M., Iacozza J., Seuthe L. and Niemi A. (2015) Arctic Ocean outflow shelves in the changing Arctic: A review and perspectives. *Prog. Oceanogr.* **139**, 66–88. Available at: http://dx.doi.org/10.1016/j.pocean.2015.08.007.

Michel C., Ingram R. G. and Harris L. R. (2006) Variability in oceanographic and ecological processes in the Canadian Arctic Archipelago. *Prog. Oceanogr.* **71**, 379–401.

Middag R., de Baar H. J. W., Klunder M. B. and Laan P. (2013) Fluxes of dissolved aluminum and manganese to the Weddell Sea and indications for manganese co-limitation. *Limnol. Oceanogr.* **58**, 287–300.

Middag R., de Baar H. J. W., Laan P., Cai P. H. and van Ooijen J. C. (2011a) Dissolved manganese in the Atlantic sector of the Southern Ocean. *Deep. Res. Part II Top. Stud. Oceanogr.* **58**, 2661–2677.

Middag R., de Baar H. J. W., Laan P. and Klunder M. B. (2011b) Fluvial and hydrothermal input of manganese into the Arctic Ocean. *Geochim. Cosmochim. Acta* **75**, 2393–2408. Available at: http://dx.doi.org/10.1016/j.gca.2011.02.011.

Middag R., van Hulten M. M. P., Van Aken H. M., Rijkenberg M. J. A., Gerringa L. J. A., Laan P. and de Baar H. J. W. (2015) Dissolved aluminium in the ocean conveyor of the West Atlantic Ocean: Effects of the biological cycle, scavenging, sediment resuspension and hydrography. *Mar. Chem.* **177**, 69–86. Available at: http://dx.doi.org/10.1016/j.marchem.2015.02.015.

Milne A., Schlosser C., Wake B. D., Achterberg E. P., Chance R., Baker A. R., Forryan A. and Lohan M. C. (2017) Particulate phases are key in controlling dissolved iron concentrations in the (sub)tropical North Atlantic. *Geophys. Res. Lett.* **44**, 2377–2387.

Moore J. K. and Braucher O. (2008) Sedimentary and mineral dust sources of dissolved iron to the world ocean To cite this version : Biogeosciences Sedimentary and mineral dust sources of dissolved iron to the world ocean. *Biogeosciences*, 631–656.

Morel F. M. M. M., Milligan A. J. and Saito M. A. (2013) *Marine Bioinorganic Chemistry: The Role of Trace Metals in the Oceanic Cycles of Major Nutrients*. 2nd ed., Elsevier Ltd. Available at: http://dx.doi.org/10.1016/B978-0-08-095975-7.00605-7.

Morel F. M. M. and Price N. M. (2003) The biogeochemical cycles of trace metals in the oceans. *Science (80-.).* **300**, 944–947.

Morgan J. J. (2005) Kinetics of reaction between O2 and Mn(II) species in aqueous solutions. *Geochim. Cosmochim. Acta* **69**, 35–48.

Nakayama Y., Fujita S., Kuma K. and Shimada K. (2011) Iron and humic-type fluorescent dissolved organic matter in the Chukchi Sea and Canada Basin of the western Arctic Ocean. *J. Geophys. Res. Ocean.* **116**, 1–16.

Nico P. S., Anastasio C. and Zasoski R. J. (2002) Rapid photo-oxidation of Mn(II) mediated by humic substances. *Geochim. Cosmochim. Acta* **66**, 4047–4056.

Nielsdóttir M. C., Moore C. M., Sanders R., Hinz D. J. and Achterberg E. P. (2009) Iron limitation of the postbloom phytoplankton communities in the Iceland Basin. *Global Biogeochem. Cycles* **23**, n/a-n/a. Available at: http://doi.wiley.com/10.1029/2008GB003410.

Nishimura S., Kuma K., Ishikawa S., Omata A. and Saitoh S. I. (2012) Iron, nutrients, and humic-type fluorescent dissolved organic matter in the northern Bering Sea shelf, Bering Strait, and Chukchi Sea. *J. Geophys. Res. Ocean.* **117**, 1–13.

Oldham V. E., Mucci A., Tebo B. M. and Luther G. W. (2017) Soluble Mn(III)–L complexes are abundant in oxygenated waters and stabilized by humic ligands. *Geochim. Cosmochim. Acta* **199**, 238–246. Available at: http://dx.doi.org/10.1016/j.gca.2016.11.043.

Parekh P., Follows M. J. and Boyle E. A. (2005) Decoupling of iron and phosphate in the global ocean. *Global Biogeochem. Cycles* **19**, n/a-n/a. Available at: http://doi.wiley.com/10.1029/2004GB002280.

Pham A. L. D. and Ito T. (2018) Formation and Maintenance of the GEOTRACES Subsurface-Dissolved Iron Maxima in an Ocean Biogeochemistry Model. *Global Biogeochem. Cycles* **32**, 932–953.

Pokrovsky O. S., Viers J., Shirokova L. S., Shevchenko V. P., Filipov A. S. and Dupré B. (2010) Dissolved, suspended, and colloidal fluxes of organic carbon, major and trace elements in the Severnaya Dvina River and its tributary. *Chem. Geol.* **273**, 136–149. Available at: http://dx.doi.org/10.1016/j.chemgeo.2010.02.018.

Proshutinsky A., Krishfield R., Timmermans M.-L., Toole J., Carmack E., McLaughlin F., Williams W. J., Zimmermann S., Itoh M. and Shimada K. (2009) Beaufort Gyre freshwater reservoir: State and variability from observations. *J. Geophys. Res.* **114**, C00A10. Available at: http://doi.wiley.com/10.1029/2008JC005104.

Richard D., Sundby B. and Mucci A. (2013) Kinetics of manganese adsorption, desorption, and oxidation in coastal marine sediments. *Limnol. Oceanogr.* **58**, 987–996.

Rijkenberg M. J. A., Middag R., Laan P., Gerringa L. J. A., Van Aken H. M., Schoemann V., De Jong J. T. M. and De Baar H. J. W. (2014) The distribution of dissolved iron in the West Atlantic Ocean.

PLoS One **9**, 1–14.

Rue E. L. and Bruland K. W. (1995) Complexation of iron(III) by natural organic ligands in the Central North Pacific as determined by a new competitive ligand equilibration/adsorptive cathodic stripping voltammetric method. *Mar. Chem.* **50**, 117–138.

Ryan-Keogh T. J., Macey A. I., Nielsdóttir M. C., Lucas M. I., Steigenberger S. S., Stinchcombe M. C., Achterberg E. P., Bibby T. S. and Moore C. M. (2013) Spatial and temporal development of phytoplankton iron stress in relation to bloom dynamics in the high-latitude North Atlantic Ocean. *Limnol. Oceanogr.* **58**, 533–545. Available at: http://doi.wiley.com/10.4319/lo.2013.58.2.0533.

Saito M. A. and Schneider D. L. (2006) Examination of precipitation chemistry and improvements in precision using the Mg(OH)2preconcentration inductively coupled plasma mass spectrometry (ICP-MS) method for high-throughput analysis of open-ocean Fe and Mn in seawater. *Anal. Chim. Acta* **565**, 222–233.

Schlitzer R., Anderson R. F., Dodas E. M., Lohan M., Geibert W., Tagliabue A., Bowie A., Jeandel C., Maldonado M. T., Landing W. M., Cockwell D., Abadie C., Abouchami W., Achterberg E. P., Agather A., Aguliar-Islas A., van Aken H. M., Andersen M., Archer C., Auro M., de Baar H. J., Baars O., Baker A. R., Bakker K., Basak C., Baskaran M., Bates N. R., Bauch D., van Beek P., Behrens M. K., Black E., Bluhm K., Bopp L., Bouman H., Bowman K., Bown J., Boyd P., Boye M., Boyle E. A., Branellec P., Bridgestock L., Brissebrat G., Browning T., Bruland K. W., Brumsack H. J., Brzezinski M., Buck C. S., Buck K. N., Buesseler K., Bull A., Butler E., Cai P., Mor P. C., Cardinal D., Carlson C., Carrasco G., Casacuberta N., Casciotti K. L., Castrillejo M., Chamizo E., Chance R., Charette M. A., Chaves J. E., Cheng H., Chever F., Christl M., Church T. M., Closset I., Colman A., Conway T. M., Cossa D., Croot P., Cullen J. T., Cutter G. A., Daniels C., Dehairs F., Deng F., Dieu H. T., Duggan B., Dulaquais G., Dumousseaud C., Echegoyen-Sanz Y., Edwards R. L., Ellwood M., Fahrbach E., Fitzsimmons J. N., Russell Flegal A., Fleisher M. Q., van de Flierdt T., Frank M., Friedrich J., Fripiat F., Fröllje H., Galer S. J. G., Gamo T., Ganeshram R. S., Garcia-Orellana J., Garcia-Solsona E., Gault-Ringold M., George E., Gerringa L. J. A., Gilbert M., Godoy J. M., Goldstein S. L., Gonzalez S. R., Grissom K., Hammerschmidt C., Hartman A., Hassler C. S., Hathorne E. C., Hatta M., Hawco N., Hayes C. T., Heimbürger L. E., Helgoe J., Heller M., Henderson G. M., Henderson P. B., van Heuven S., Ho P., Horner T. J., Hsieh Y. Te, Huang K. F., Humphreys M. P., Isshiki K., Jacquot J. E., Janssen D. J., Jenkins W. J., John S., Jones E. M., Jones J. L., Kadko D. C., Kayser R., Kenna T. C., Khondoker R., Kim T., Kipp L., Klar J. K., Klunder M., Kretschmer S., Kumamoto Y., Laan P., Labatut M., Lacan F., Lam P. J., Lambelet M., Lamborg C. H., Le Moigne F. A. C., Le Roy E., Lechtenfeld O. J., Lee J. M., Lherminier P., Little S., López-Lora M., Lu Y., Masque P., Mawji E., Mcclain C. R., Measures C., Mehic S., Barraqueta J. L. M., van der Merwe P., Middag R., Mieruch S., Milne A., Minami T., Moffett J. W., Moncoiffe G., Moore W. S., Morris P. J., Morton P. L., Nakaguchi Y., Nakayama N., Niedermiller J., Nishioka J., Nishiuchi A., Noble A., Obata H., Ober S., Ohnemus D. C., van Ooijen J., O'Sullivan J., Owens S., Pahnke K., Paul M., Pavia F., Pena L. D., Peters B., Planchon F., Planquette H., Pradoux C., Puigcorbé V., Quay P., Queroue F., Radic A., Rauschenberg S., Rehkämper M., Rember R., Remenyi T., Resing J. A., Rickli J., Rigaud S., Rijkenberg M. J. A., Rintoul S., Robinson L. F., Roca-Martí M., Rodellas V., Roeske T., Rolison J. M., Rosenberg M., Roshan S., Rutgers van der Loeff M. M., Ryabenko E., Saito M. A., Salt L. A., Sanial V., Sarthou G., Schallenberg C., Schauer U., Scher H., Schlosser C., Schnetger B., Scott P., Sedwick P. N., Semiletov I., Shelley R., Sherrell R. M., Shiller A. M., Sigman D. M., Singh S. K., Slagter H. A., Slater E., Smethie W. M., Snaith H., Sohrin Y., Sohst B., Sonke J. E., Speich S., Steinfeldt R., Stewart G., Stichel T., Stirling C. H., Stutsman J., Swarr G. J., Swift J. H., Thomas A., Thorne K., Till C. P., Till R., Townsend A. T., Townsend E., Tuerena R., Twining B. S., Vance D., Velazquez S., Venchiarutti C., Villa-Alfageme M., Vivancos S. M., Voelker A. H. L., Wake B., Warner M. J., Watson R., van Weerlee E.,

Alexandra Weigand M., Weinstein Y., Weiss D., Wisotzki A., Woodward E. M. S., Wu J., Wu Y., Wuttig K., Wyatt N., Xiang Y., Xie R. C., Xue Z., Yoshikawa H., Zhang J., Zhang P., Zhao Y., Zheng L., Zheng X. Y., Zieringer M., Zimmer L. A., Ziveri P., Zunino P. and Zurbrick C. (2018) The GEOTRACES Intermediate Data Product 2017. *Chem. Geol.* **493**, 210–223.

Shelley R. U., Landing W. M., Ussher S. J., Planquette H. and Sarthou G. (2018) Regional trends in the fractional solubility of Fe and other metals from North Atlantic aerosols (GEOTRACES cruises GA01 and GA03) following a two-stage leach. *Biogeosciences* **15**, 2271–2288.

Shimada K., Itoh M., Nishino S., McLaughlin F., Carmack E. and Proshutinsky A. (2005) Halocline structure in the Canada Basin of the Arctic Ocean. *Geophys. Res. Lett.* **32**, 1–5.

Sim N. (2018) Biogeochemical cycling of dissolved and particulate manganese in the northeast Pacific and Canadian western Arctic. University of British Columbia. Available at: https://open.library.ubc.ca/cIRcle/collections/ubctheses/24/items/1.0374222.

Smethie W. M., Schlosser P., Bönisch G. and Hopkins T. S. (2000) Renewal and circulation of intermediate waters in the Canadian Basin observed on the SCICEX 96 cruise. *J. Geophys. Res. Ocean.* **105**, 1105–1121.

Statham P. J., Yeats P. A. and Landing W. M. (1998) Manganese in the eastern Atlantic Ocean: Processes influencing deep and surface water distributions. *Mar. Chem.* **61**, 55–68.

Steele M., Morison J., Ermold W., Rigor I., Ortmeyer M. and Shimada K. (2004) Circulation of summer Pacific halocline water in the Arctic Ocean. *J. Geophys. Res.* **109**, 1–18. Available at: http://doi.wiley.com/10.1029/2003JC002009.

Sunda W. G. (1997) Control of dissolved iron concentrations in the world ocean: A comment. *Mar. Chem.* **57**, 169–172.

Sunda W. G. and Huntsman S. A. (1994) Photoreduction of manganese oxides in seawater. *Mar. Chem.* **46**, 133–152.

Sunda W. G., Huntsman S. A. and Harvey G. R. (1983) Photoreduction of manganese oxides in seawater and its geochemical and biological implications. *Nature* **301**, 234–236.

Tagliabue A., Bowie A. R., Boyd P. W., Buck K. N., Johnson K. S., Saito M. A., Philip W., Buck K. N., Johnson K. S. and Saito M. A. (2017) The integral role of iron in ocean biogeochemistry. *Nature* **543**, 51–59. Available at: http://dx.doi.org/10.1038/nature21058.

Tang C. C. L., Ross C. K., Yao T., Petrie B., DeTracey B. M. and Dunlap E. (2004) The circulation, water masses and sea-ice of Baffin Bay. *Prog. Oceanogr.* **63**, 183–228.

Tanhua T., Jones E. P., Jeansson E., Jutterström S., Smethie W. M., Wallace D. W. R. and Anderson L. G. (2009) Ventilation of the arctic ocean: Mean ages and inventories of anthropogenic CO2 and CFC-11. *J. Geophys. Res. Ocean.* **114**, 1–11.

Thuróczy C. E., Gerringa L. J. A., Klunder M., Laan P., Le Guitton M. and De Baar H. J. W. (2011) Distinct trends in the speciation of iron between the shallow shelf seas and the deep basins of the Arctic Ocean. *J. Geophys. Res. Ocean.* **116**, 1–21.

Timmermans M. L., Garrett C. and Carmack E. (2003) The thermohaline structure and evolution of the deep waters in the Canada Basin, Arctic Ocean. *Deep. Res. Part I Oceanogr. Res. Pap.* **50**, 1305–1321.

Timmermans M. L., Marshall J., Proshutinsky A. and Scott J. (2017) Seasonally derived components of the Canada Basin halocline. *Geophys. Res. Lett.* **44**, 5008–5015.

Top Z., Clarke W. B., Eismont W. C. and Jones E. P. (1980) Radiogenic helium in Baffin Bay bottom water. *J. Mar. Res.* **38**, 435–452.

Tortell P. D., Maldonado M. T. and Price N. M. (1996) The role of heterotrophic bacteria in iron-limited ocean ecosystems. *Nature* **383**, 330–332.

Varela D. E., Crawford D. W., Wrohan I. A., Wyatt S. N. and Carmack E. C. (2013) Pelagic primary productivity and upper ocean nutrient dynamics across Subarctic and Arctic Seas. *J. Geophys. Res. Ocean.* **118**, 7132–7152.

Vieira L. H., Achterberg E. P., Scholten J., Beck A. J., Liebetrau V., Mills M. M. and Arrigo K. R. (2019) Benthic fluxes of trace metals in the Chukchi Sea and their transport into the Arctic Ocean. *Mar. Chem.* **208**, 43–55. Available at: https://linkinghub.elsevier.com/retrieve/pii/S0304420318301282.

Wang Q., Myers P. G., Hu X. and Bush A. B. G. (2012) Flow constraints on pathways through the Canadian Arctic archipelago. *Atmos. - Ocean* **50**, 373–385.

Weiss R. F. (1977) Hydrothermal manganese in the deep sea: Scavenging residence time and Mn/3He relationships. *Earth Planet. Sci. Lett.* **37**, 257–262.

Woodgate R. A. and Aagaard K. (2005) Revising the Bering Strait freshwater flux into the Arctic Ocean. *Geophys. Res. Lett.* **32**, 1–4.

Wu J. and Boyle E. A. (1998) Determination of iron in seawater by high-resolution isotope dilution by high-resolution inductively coupled plasma mass spectrometry after Mg(OH)2 coprecipitation. *Anal. Chim. Acta* **367**, 183–191.

Wu J. F., Boyle E., Sunda W. and Wen L. S. (2001) Soluble and colloidal iron in the olgotrophic North Atlantic and North Pacific. *Science (80-.).* **293**, 847–849.

Wu J., Roshan S. and Chen G. (2014) The distribution of dissolved manganese in the tropical-subtropical North Atlantic during US GEOTRACES 2010 and 2011 cruises. *Mar. Chem.* **166**, 9–24. Available at: http://dx.doi.org/10.1016/j.marchem.2014.08.007.

Wu J., Wells M. L. and Rember R. (2011) Dissolved iron anomaly in the deep tropical-subtropical Pacific: Evidence for long-range transport of hydrothermal iron. *Geochim. Cosmochim. Acta* **75**, 460–468. Available at: http://dx.doi.org/10.1016/j.gca.2010.10.024.

Yashayaev I., Bersch M. and van Aken H. M. (2007) Spreading of the Labrador Sea Water to the Irminger and Iceland basins. *Geophys. Res. Lett.* **34**, 1–8.

Yashayaev I. and Clarke A. (2008) Evolution of North Atlantic Water Masses Inferred from Labrador Sea Salinity Series. *Oceanography* **21**, 30–45.

Yashayaev I. and Loder J. W. (2009) Enhanced production of Labrador Sea Water in 2008. *Geophys. Res. Lett.* **36**, L01606.

Yashayaev I. and Loder J. W. (2016) Recurrent replenishment of Labrador Sea Water and associtated decadal-scale variability. *J. Geophys. Res. Ocean.* **121**, 8095–8114.

Yeats P. A. and Bewers J. M. (1985) Manganese in the Western North Atlantic Ocean. *Mar. Chem.* **17**,

255–263.